Comparing Geometric Models Against Empirical Data for Radiowave Landmobile Cellular Uplink AOA

by

Minaz Abdulla

A thesis
presented to the University of Waterloo
in fulfillment of the
thesis requirement for the degree of
Master of Applied Science
in
Electrical and Computer Engineering

Waterloo, Ontario, Canada, 2005

I hereby declare that I am the sole author of this thesis. This is a true copy of the thesis, including any required final revisions, as accepted by my examiners.

I understand that my thesis may be made electronically available to the public.

Minaz Abdulla

Abstract

There has been an increase in demand for efficient wireless systems. Smart antennas using position location are one possible way to improve the capacity of cellular systems. In order to deploy such systems successfully, the wireless network must properly exploit the processing of spatial information (ie. The uplink angle of arrival) through wireless channel models.

Geometric modelling is a technique to model the wireless environment. When compared to other methods such as ray tracing simulations, geometric models allow one to classify a wide varity of environments within a single model.

Secondly, there have been much research in the past to obtain empirical measurements in many different environment settings. These measurements have been recorded, however, there has been no research undertaken to systematically compare and validate the empirical findings with current geometric models. The goal of this research is to compare and constrast geometric models with empirical data in order to show which models are best suited for specific wireless environments. The uplink angle of arrival (AOA) probability distribution is the fading metric that will be used to compare and contrast these models.

Acknowledgements

First of all, I would like to thank my supervisor, Prof. K. T. Wong for taking me on as his graduate student. He has helped and guided me throughout my entire research here at the University of Waterloo.

Secondly, I would like to thank my family and friends for supporting me throughout my studies and research, as I would not have been able to done it without you!

Contents

1 Background **1**

1.1 What is Small Scale Fading ? 1

1.2 Uplink Angle of Arrival 4

1.3 Smart Antenna Systems 4

2 Modeling Wireless Fading Channels **7**

2.1 Introduction 7

2.2 Ray Tracing Models 7

2.2.1 Geometric Models 8

2.2.2 Ad Hoc Models 8

2.2.3 Geometric vs Ad Hoc 9

2.2.4 Geometric vs Ray Tracing 9

2.2.5 Model Summary 10

3 Analytically Derived TOA-DOA Statistics for Inverted-Parabola **12**

3.1 Overview 12

3.2 Assumptions 12

3.3 Uplink's AOA-TOA Joint Distribution 15

3.4 Uplink's AOA Marginal Distribution 16
3.5 TOA Marginal Distribution 17
3.6 Downlink's Multipaths' TOA-AOA Distributions 18

4 Compare and Contrast of Geometric Models **20**

5 Compare and Contrast of Empirical Data **34**
5.1 Least-Square-Error Fitting of AOA models 34
5.1.1 Empirical Measurement Environment Settings 38
5.1.2 Conclusions 41

A Rayleigh vs Gaussian Scatterer Distributions **53**

B AOA Distribution Fitting using AOA spread **55**

C TOA Distributions **58**
C.0.3 TOA models vs empirical data 59

List of Tables

2.1 Advantages and Diadvantages of Modeling Techniques 11

4.1 Probability density functions for "Geometrical Models" 22
4.2 Summary of DOA distribution curve parameters 31

5.1 Least-Square Errors for "Geometrical Models" with empirical datatsets . . 37
5.2 Propagation and Measurement Environment for empirical datatsets 40
5.3 Best three models compared against empirical datatsets 41

B.1 Parameters corresponding to angular spread for "Geometrical Models" . . 55

C.1 Parameters corresponding to delay spread for "Geometrical Models" 60

List of Figures

1.1 Large Scale and Small Scale Fading 3

1.2 Omni-direction BaseStation vs Smart Antenna BaseStation 6

3.1 The Geometry Relating the Mobile, the Scatterers, and the Base Station . 14

3.2 The Scatterers' "Inverted Parabolic" Spatial Density, D = 1km, R = 0.3km 14

3.3 $f_{\tau,\theta_u}(\tau,\theta_u)$, at $R = 100$ meters and $D = 1000$ meters. 16

3.4 $f_{\tau,\theta_d}(\tau,\theta_d)$, at $R = 100$ meters and $D = 1000$ meters. 19

4.1 AOA distribution for all geometric models 29

5.1a KavakAsilomar98 43

5.1b KlochAPT0901 43

5.1c LaurilaAPT0202 43

5.1d MatthewsICMPRC89 43

5.2a KleinISSSTA96 44

5.2b KleinISSSTA96 44

5.2c KleinISSSTA96 44

5.2d PedersenVTC98 44

5.3a PedersenVTT0300 45

5.3b TakadaJSAC0402 45

5.3c TanakaJSAC0800 45
5.3d ThomaIMT0400 45
5.4a ZhaoJSAC0402 46
5.4b ZhuAPSIS00 46
5.4c ZhuVTC01S 46

A.1a Rayleigh vs Gaussian Distribution for $D/\sigma = 1$ 54
A.1b LSE for various values of D/σ 54

B.1a AOA KlochAPT0901 56
B.1b AOA FleuryJSAC0399 56
B.1c AOA LaurilaAPT0202 57
B.1d AOA PedersenVTT0300 57
B.1e AOA TanakaJSAC0800 57
B.1f AOA ThomaIMT0400 57

C.1a TOA PedersonVTT0300 $D = 1500$ 60
C.1b TOA PedersonVTT0300 $D = 1750$ 60
C.1c TOA PedersonVTT0300 $D = 2000$ 61
C.1d TOA KlochAPT0901 61
C.2a TOA KucharAPT0200 62
C.2b TOA LaurilaAPT0202 62
C.2c TOA ErcegJSAC0399 $D = 500$ 62
C.2d TOA SteinbauerAPT0801 Scenario 2.eps 62
C.3a TOA SteinbauerAPT0801 Scenario 3.eps 63
C.3b TOA SteinbauerAPT0801 Scenario 4.eps 63

Chapter 1

Background

1.1 What is Small Scale Fading ?

In a perfect communication channel, attenuation of a wireless signal over a distance occurs in free space. The objects or obstacles in between the transmitter and receiver do not absorb or reflect any of the signals energy. The atmosphere also exhibits this same behaviour.

However, in a real world scenario, such an environment is not possible. A signal transmitted from a mobile user gets corrupted with random noise and is also received at the receiver via multiple propagation paths. [1] These results in a signal that is reflected, diffracted, and scattered multiple times before reaching the final destination. The receiving data measurement of each antenna represents the summed effect of these individually unobservable multipaths. However, when the multipaths are summed, they may contain different phase values. These phase differences (as tiny as a half wavelength) can degrade

[1] A multipath carries its own propagation history of electromagnetic reflections and diffractions and corruption by multiplicative noise. A history represents the multipaths amplitude, Doppler, arrival angle, and arrival time delay at the receiving antenna.

or even cancel the received signal. This is known as small scale fading. When the signal is cancelled due to multipath fading, the signal is said to be in a deep fade.

Secondly, since the local scatterers reflect the signal many times, the transmitted signal travels to the receiver via multiple paths, each having their own associated path length. This results in the signal arriving at the receiver at various time delays. Time delays in the signal result in time dispersion or spreading of the signal. This is also known as a time-varying wireless channel. If the arrival delay is larger than the symbol interval, the signal will overlap with other symbols. This is known as inter-symbol interference (ISI). In another words, the channel characteristics change faster than time required to receive one complete period of signal. Therefore, the complex channel gain is not constant over the entire symbol interval. ISI is one major factor in increasing the bit error rate (BER).

When there exists a line of sight (LOS) between the transmitter and receiver, the small-scale fading is statistically modeled by a Rician probability distribution. If no line of sight (NLOS) exits, a Rayleigh distribution is used to model the fading behaviour.

Another type of fading is called large-scale fading. Large-scale fading represents the average signal power attenuation or the path loss due to motion over large areas. This phenomenon is affected by dominant terrain contours such as hills, forests, buildings, etc. The receiver is often said to be shadowed by such obstacles. The statistics of large-scale fading provide a way of computing an estimation of path loss as a function of the distance. This is described in terms of a mean-path loss (nth-power law) and a log-normally distributed variation about the mean.

Figure 1.1 shows the typical signal power received at a mobile unit. We can break up the signal into multiple components: path loss, shadowing, and small scale fading. Due to the scope of this research, the mathematical analysis in this thesis will focus only on the microscopic (small scale) fading statistics, not macroscopic (large scale) statistics such as

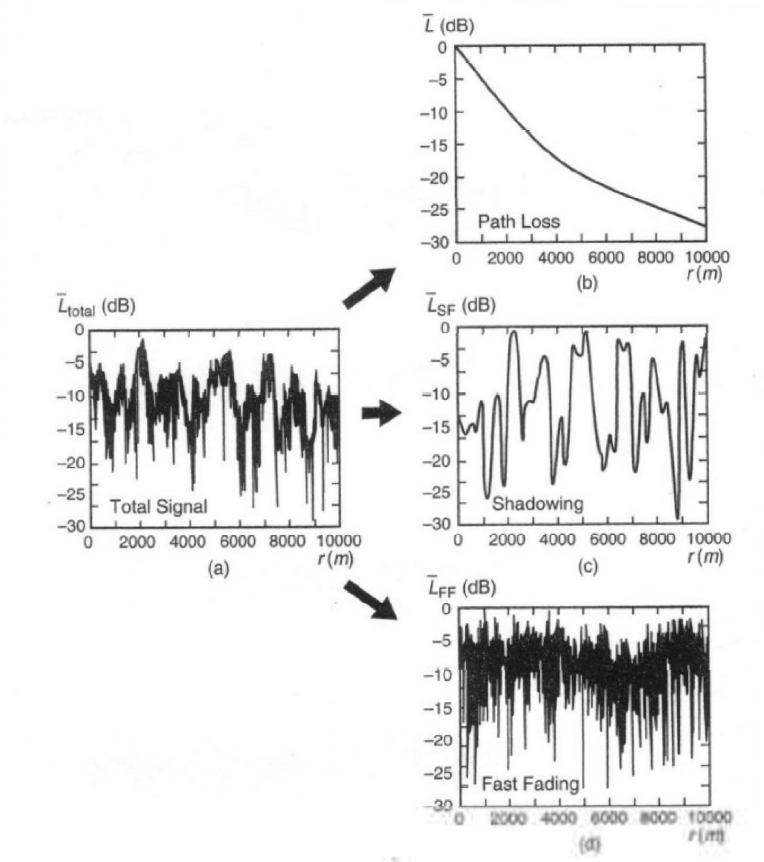

Figure 1.1: Large Scale and Small Scale Fading

that due to shadowing.

1.2 Uplink Angle of Arrival

Small-scale fading is a result of scattering multipaths in a wireless channel environment. Due to the local scatterers around the mobile unit, the signal will be reflect in all directions. As a result, the signals multipaths will arrive at the mobile stations receiving antenna from many of these angular directions. These angles are known as the angle of arrival (AOA). If we were to normalize the power received in this angular domain, we can then generate a probability distribution function. In another words, the AOA is a scaled version of the probability density function (pdf) in the angular domain.

There are many applications within wireless communications that exploit the use of angular statistics. One such application is with adaptive or smart antennas systems. The AOA is the most crucial component that these systems rely on.

1.3 Smart Antenna Systems

The recent tremendous growth in wireless communications has led to crowding or overloading of the radio spectrum. Current wireless systems can not handle this increasing load as they are designed to be inefficient. Systems today use omni-directions antennas at the base station. The signal that is transmitted is sent out in all directions as shown in Figure 1.2. Therefore, only a small percentage of the total signal transmitted reached the mobile user. Another problem resulting from omni-directional antennas is co-channel interference. This occurs when neighboring cells overlap each others frequency spectrum resulting in interference. In another words, the same carrier frequency reaches the one user from two separate transmitting cells causing interference.

Traditionally, to overcome such problems, cell splitting has been used to cope up with the increase in the number of users in a cellular system. Cell splitting increases the capacity

of a cellular system by subdividing or splitting cells into two or more smaller cells. However, cell splitting is expensive and requires reconfiguring the cellular network.

Smart antenna systems are the new alternative to currently deployed systems. Smart antenna systems attempt to overcome the current problems of inefficiency and capacity. Instead of using omni-directional antenna's, the base stations use directional antennas to focus the signal energy towards the mobile unit as shown in Figure 1.2. By using the AOA statistics of the wireless channel, the base station can locate the direction of the mobile unit. As a result, smart antenna systems can provide the following advantages:

- Suppression of co-channel interference due to reduced multipath propagation.
- Increased signal gain
- Increased range or coverage within cell.
- Spectral efficiency by mobile localization and multiple diversity schemes. Diversity schemes involve recombining the information from multipath components of signals with lower bit error rates while still using lower transmitting power.

In order for smart antenna systems to be deployed in the field, there needs to be a thorough understanding of the wireless propagation phenomena. Many models in the past have described the received field strength, the power delay profiles, and the Doppler spectra. Although these parameters are important for the analysis of systems with omni-directional antennas, new smart antenna systems require knowledge of angle of arrival (AOA) statistics. Using the angle of arrival metrics, the system can be designed to exploit this spatial information to improve the efficiency of the wireless system. Models in the past are unable to derive such statistics due to the fact that the Doppler spectra are dependent on the velocity and direction of motion of scatterers and the mobile station. Therefore,

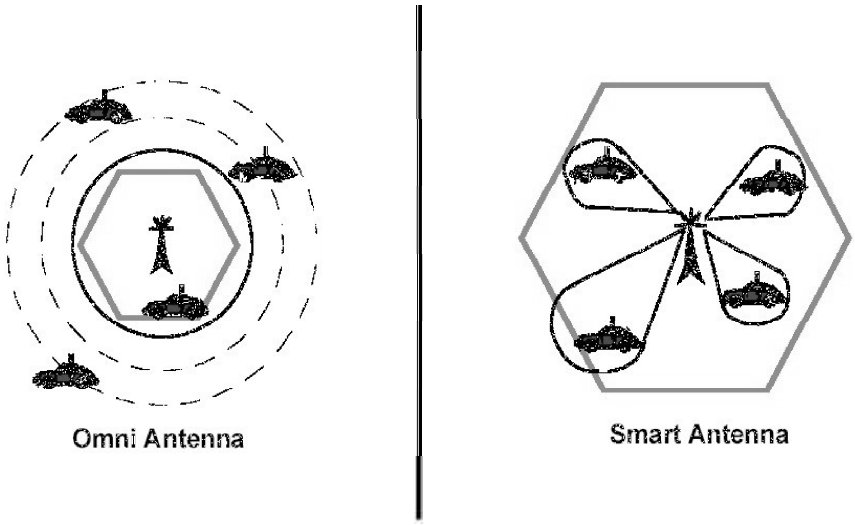

Figure 1.2: Omni-direction BaseStation vs Smart Antenna BaseStation

the realistic design and simulation of smart antenna systems requires new accurate spatial channel models. It is for this reason that there has been a motivation for developing new models.

Chapter 2

Modeling Wireless Fading Channels

2.1 Introduction

It is important to model small scale fading and its affect on performance in order for smart antenna systems to be deployed. The modeling of this type of communication system requires a statistical modeling of the wireless channel and its angular statistics. Various methods for modeling such an environment exist today. The most common modeling techniques are Geometric modeling, Ad-hoc modeling, and Ray-tracing modeling. Each of these modeling techniques will be discussed and compared, however the focus of this report will concentrate on geometric modeling.

2.2 Ray Tracing Models

Ray-tracing modeling (based on electromagnetic modeling) is unique in the sense that it retains the full (or almost the full) electromagnetic and spatio-temporal complexities of the specific propagation channel under investigation. The analysis of this model can be

achieved through electromagnetic-physics-based analysis or can be achieved through ray-tracing computer simulations. Its quantitative accuracy makes this type of modeling very advantageous. However, new simulations must be performed for each specific environment setting (ie downtown, rural, etc). Therefore, this dependency for particular environment settings does not make it feasible to be applicable to a much wider class of propagation settings.

2.2.1 Geometric Models

Another type of modeling, called Geometric modeling, refers to a mathematically rigorous derivation of the received signal's measurable statistical properties. This is achieved through geometric abstraction of the wireless environment. The geometric abstraction involves the use of spatial relationships between the transmitter, receiver and all local scatterers. The mathematical derivation is integrated based on an idealization of the spatial geometry that is altogether simple, generic (i.e. site non-specific) and abstract. The geometric parameters that would affect the fading metrics are inter-connected in a way that will result in representing the channel's underlying fading dynamics. Secondly, the generic abstract geometry of this model involves no site-specific, terrain-specific, or building-specific information such as those used in empirical measurements or in ray-shooting. This makes geometric modeling high advantageous.

2.2.2 Ad Hoc Models

There is no specific example of an Ad hoc model, however, as its name implies, these models consists of all models that are conceived without any rigorous research. They are simply made up out of thin air. They involve no (or very little) mathematical derivation and do not perform any simulations to obtain results.

2.2.3 Geometric vs Ad Hoc

Geometric modeling can be contrasted with ad hoc non-geometric models. Ad Hoc models may impose certain improvised and a priori statistics. These statistics correspond to the individual aspects of the multipaths' spatial and temporal behavior without embedding any side-by-side presumptions into an integrated comprehensive model. This results in no underlying geometric inter-connection among the model and its other fading metrics. Such models demonstrate very little or no analytical insight into the propagation channel's fundamental dynamics. As a result, it is difficult to generalize any meaningful data due to a missing fundamental framework. There is also no framework to allow meaningful generalization into categorically different propagation settings such as that provided with geometric models.

2.2.4 Geometric vs Ray Tracing

Geometric modeling contrasts with site-specific, terrain-specific or building-specific empirical measurements obtained from exhaustive ray-shooting / ray-tracing computer simulations. These simulations which are applicable only to the one particular propagation setting under investigation cannot be easily generalized to wider scenarios. A benefit is that one geometric model can apply for a wide class of propagation settings. This produces the received-signal's measurable fading metrics (e.g. the uplink and downlink probability density functions of the multipaths' arrival delay and two-dimensional arrival angle) that can be then applicable more generically within that class of channels.

Given a model's set of inter-relations (such as spatial distance, LOS, elevation, etc), which correspond to the mobile, the scatterers and the base station, the channel fading metrics could be estimated through numerical approximations of the Monte Carlo [1] simu-

[1]The Monte Carlo simulation provides approximate solutions to a variety of mathematical problems by

lations as in [1], [2], [9], [13], [14], [19], [22]. However, this can not produce a closed-form expression of the fading statistics through the geometric-model's independent parameters. Therefore, this limits the knowledge obtainable from such a model.

Ray tracing channel models, which are based on the complete description of the field environments, are not practical due to the field conditions complexity and variability. Consider the following example. The received power at a cellular base-station depends on the electromagnetic response of the base-station's receiving antennas. As many urban cellular base-stations are built on roof-tops, unpredictable happenings such as the passing of a truck or bus or the signal from a neighbor's newly constructed TV antenna could distort the base-station antennas' response considerably. An electromagnetic analysis starting from the Maxwell's equations would involve a difficult large number of independent variables.

2.2.5 Model Summary

Most "geometric models" involve little or no rigorous mathematical derivation of the received signal's measurable fading statistics. This is due to the inherent mathematical difficulties when deriving such models. Instead, such models would perform a limited series of Monte Carlo computer-simulation experiments based on the "geometric models". Many models, of course, lie somewhere in the middle. For example, there are many research initiatives that involve an incomplete mathematical analysis which result in open-form expressions of the fading statistics. These results have unsolved complex summations or integrals, which are estimated for a few sample propagation channels through limited Monte Carlo computer-simulation experiments. Instead, the present work takes a longer and tough path, yet more productive path of a mathematical analysis in order to obtain close-form explicit expressions of the wireless environments statistical metrics. The follow-

performing statistical sampling experiments.

ing table is a summary of the advantages and disadvantages of the models discussed in this section.

Model Type	Advantages	Disadvantages
Ad Hoc	-Simple (no derivation or simulation)	-A priori knowledge is required. -No insight into the propagation-channel's fundamental dynamics
Ray Tracing	-Very accurate quantitative analysis	-Applicable to one particular propagation setting -Not practical due to the field conditions complexity and variability
Geometric	-Can apply for a wide class of propagation settings -Underlying geometric inter-connection on its other fading metrics -Rigorously derived closed-form expressions -Integrated and comprehensive conceptual foundation for an entire class of fading-channels' underlying propagation mechanism	-Low degree of accuracy for any specific field environment as compared against site specific

Table 2.1: Advantages and Diadvantages of Modeling Techniques

Chapter 3

Analytically Derived TOA-DOA Statistics for Inverted-Parabola

3.1 Overview

In the past, there have been many rigorously derived closed-form explicit expressions to model the wireless cellular multipaths delay and angle of arrival (TOA-AOA) statistics. A new geometric model is derived in this section such that the scatterers are assumed to have an inverted-parabolic spatial distribution on a two-dimensional disc centered around the mobile station.

3.2 Assumptions

From Figure 3.1, we formulate the two-dimensional geometry in order to derive the joint and marginal TOA and AOA pdfs. For simplicity, only one scatterer is shown and its relation to the Mobile Station and Base Station. The scatterers in this geometry have

an inverted parabolic spatial distribution as seen in Figure 3.2, where D represents the distance from the MS to the BS, and R represents the radius of the disc centered around the MS. From these figures, we can make the following assumptions:

1) All transmitting and receiving antennas are omni directional.

2) Polarization effects may be ignored.

3) Each propagation path, from the mobile to the base-station, reflects off exactly one scatterer.

4) Each scatterer acts (independently of other scatterers) as an omni directional lossless re-transmitter.

5) Scatterers are randomly located with a Cartesian "inverted parabolic" spatial density $f_{x,y}(x,y) =$

$$\begin{cases} \frac{2}{\pi R^2}\left[1-\frac{(x-D)^2+y^2}{R^2}\right], & \text{if } (x-D)^2+y^2 \leq R^2 \\ 0, & \text{otherwise} \end{cases} \tag{3.1}$$

Hence, the scatterers are confined to only a finite two-dimensional disc-like spatial support-region, centered around the mobile transmitter at $(x = D, y = 0)$. See Figure 3.2.

6) Negligible complex-phase effects in the receiving antenna's vector-summation of its arriving multipaths. That is, all arriving multipaths arriving at each receiving-antenna are assumed to be temporally in-phase among themselves.

The inverted parabolic spatial density indirectly accounts for scattering power loss, as opposed to the "uniform circular disc" or the uniform hollow-disc density derived in ([4], [5], [7], [8], [17], [20]), and [24]. Scattering power loss is accounted for by having a

lower spatial density of scatterers for spatial regions where the propagation paths are likely to have reflection power loss. In another words, it assumes more frequent reflections off scatterers nearer to the mobile than scatterers further away. This is accurate of a real world scenario because a reflection farther from the mobile will be severely more degraded due to multiple reflections (without first reaching the mobile station) that occur farther away from the mobile.

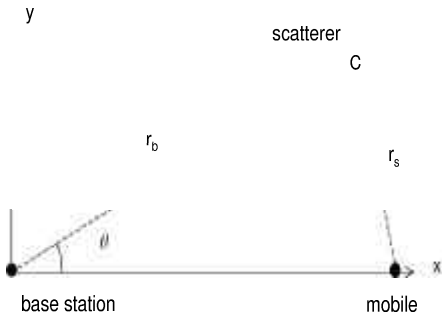

Figure 3.1: The Geometry Relating the Mobile, the Scatterers, and the Base Station

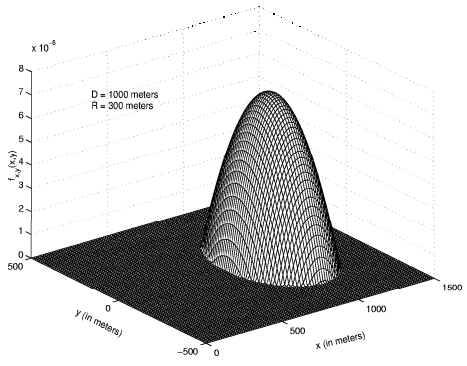

Figure 3.2: The Scatterers' "Inverted Parabolic" Spatial Density, D = 1km, R = 0.3km

3.3 Uplink's AOA-TOA Joint Distribution

The scatterers' spatial distribution's support region, in terms of the geometry in Figure 3.1, equals:

$$R^2 \geq (r_b \cos\theta_u - D)^2 + (r_b \sin\theta_u)^2 \tag{3.2}$$

and $r_b = \frac{D^2-\tau^2c^2}{2(D\cos\theta_u - \tau c)}$. The scatterers' Cartesian spatial density in (3.1) may be expressed in terms of the multipaths' TOA-AOA (τ, θ_u) arriving at the cellular basestation through a Jacobian transformation [17], When (3.2) holds,

$$f_{\tau,\theta_u}(\tau,\theta_u) = \frac{cD(1-\left(\frac{\tau c}{D}\right)^2)\left[1+\left(\frac{\tau c}{D}\right)^2 - 2\frac{\tau c}{D}\cos\theta_u\right]}{4\left(\cos\theta_u - \frac{\tau c}{D}\right)^3} \underbrace{\frac{2}{\pi R^2}\left[1 - \frac{(r_b\cos\theta_u - D)^2 + (r_b\sin\theta_u)^2}{R^2}\right]}_{=f_{x,y}(r_b\cos\theta_u, r_b\sin\theta_u)}$$

$$= \frac{c}{2\pi D}\left(\frac{R}{D}\right)^{-4} \frac{\left[1-\left(\frac{\tau c}{D}\right)^2\right]\left[1+\left(\frac{\tau c}{D}\right)^2 - 2\frac{\tau c}{D}\cos\theta_u\right]}{\left(\cos\theta_u - \frac{\tau c}{D}\right)^3}$$
$$\left\{\left(\frac{R}{D}\right)^2 - 1 - \left[\frac{1-(\frac{\tau c}{D})^2}{2(\cos\theta_u - \frac{\tau c}{D})}\right]^2 + \frac{\left[1-\left(\frac{\tau c}{D}\right)^2\right]\cos\theta_u}{\cos\theta_u - \frac{\tau c}{D}}\right\}$$

and $f_{\tau,\theta_u}(\tau,\theta_u) = 0$ when (3.2) is false. Figure 3.3 plots $f_{\tau,\theta_u}(\tau,\theta_u)$ for $R = 100$ meters and $D = 1000$ meters.

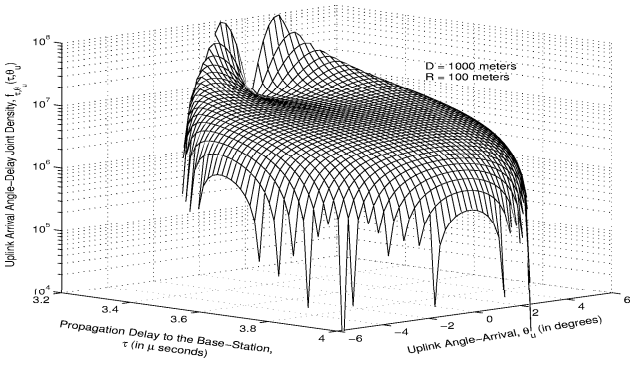

Figure 3.3: $f_{\tau,\theta_u}(\tau,\theta_u)$, at $R = 100$ meters and $D = 1000$ meters.

3.4 Uplink's AOA Marginal Distribution

Restriction (3.2) requires r_b to lie between $D\left(\cos\theta_u \pm \sqrt{(\frac{R}{D})^2 - \sin^2\theta_u}\right)$ [17]. The Jacobian transformation [17] $\frac{f_{r_b,\theta_u}(r_b,\theta_u)}{r_b} = f_{x,y}\left(r_b\cos\theta_u, r_b\sin\theta_u\right)$ leads to:

$$f_{\theta_u}(\theta_u) = \int_{\frac{D}{c}}^{\frac{D+2R}{c}} f_{\tau,\theta_u}(\tau,\theta_u)d\tau$$

$$\begin{aligned} &= \int_{D\left(\cos\theta_u-\sqrt{(\frac{R}{D})^2-\sin^2\theta_u}\right)}^{D\left(\cos\theta_u+\sqrt{(\frac{R}{D})^2-\sin^2\theta_u}\right)} r_b f_{x,y}(r_b\cos\theta_u, r_b\sin\theta_u)dr_b \\ &= \frac{8\cos\theta_u}{3\pi}\left(\frac{R}{D}\right)^{-4}\left[\left(\frac{R}{D}\right)^2 - \sin^2\theta_u\right]^{3/2} \end{aligned} \tag{3.3}$$

for $\theta_u \in \left[-\arcsin\frac{R}{D}, \arcsin\frac{R}{D}\right]$; otherwise, $f_{\theta_u}(\theta_u) = 0$. The symmetry of $f_{\theta_u}(\theta_u)$ with respect to $\theta_u = 0$ implies $\mathrm{E}[\theta_u] = 0$.

3.5 TOA Marginal Distribution

Any two-dimensional constant-τ curve may intersect with the scatterers' support region's border at most twice. Because of (3.2) and $\tau c = r_b + R$, the integration limits θ_1 and θ_2 in:

$$f_\tau(\tau) \;=\; \int_{-\pi}^{\pi} f_{\tau,\theta_u}(\tau,\theta_u)d\theta_u$$

$$= \int_{\theta_1}^{\theta_2} \frac{cD(1-\left(\frac{\tau c}{D}\right)^2)\left[1+\left(\frac{\tau c}{D}\right)^2-2\frac{\tau c}{D}\cos\theta_u\right]}{4\left(\cos\theta_u-\frac{\tau c}{D}\right)^3} f_{x,y}\left(\frac{(1-\left(\frac{\tau c}{D}\right)^2)}{2(\cos\theta_u-\frac{\tau c}{D})}D\cos\theta_u, \frac{(1-\left(\frac{\tau c}{D}\right)^2)}{2(\cos\theta_u-\frac{\tau c}{D})}D\sin\theta_u\right)d\theta_u$$

equal $\mp\arccos\left(\frac{(\frac{\tau c}{D})^2+1-2\frac{\tau c}{D}\frac{R}{D}}{2(\frac{\tau c}{D}-\frac{R}{D})}\right)$. Hence,

$$f_\tau(\tau) = \frac{c}{\pi D}\left[1-\left(\frac{\tau c}{D}\right)^2\right](\frac{R}{D})^{-4}\int_0^{\theta_2} d\theta_u \frac{1+\left(\frac{\tau c}{D}\right)^2-2\frac{\tau c}{D}\cos\theta_u}{\left(\cos\theta_u-\frac{\tau c}{D}\right)^3} \left\{(\frac{R}{D})^2-1-\left[\frac{1-\left(\frac{\tau c}{D}\right)^2}{2(\cos(\theta_u)-\frac{\tau c}{D})}\right]^2+\frac{(1-\left(\frac{\tau c}{D}\right)^2)\cos(\theta_u)}{\cos(\theta_u)-\frac{\tau c}{D}}\right\}$$

$$= \frac{2c}{\pi D}\left[1-\left(\frac{\tau c}{D}\right)^2\right](\frac{R}{D})^{-4}\int_0^{x_1} \frac{dx}{1+x^2}\frac{1+\left(\frac{\tau c}{D}\right)^2-2\frac{\tau c}{D}\frac{1-x^2}{1+x^2}}{\left[\left(\frac{1-x^2}{1+x^2}\right)-\frac{\tau c}{D}\right]^3} \left\{(\frac{R}{D})^2-1-\left[\frac{1-\left(\frac{\tau c}{D}\right)^2}{2\left(\frac{1-x^2}{1+x^2}-\frac{\tau c}{D}\right)}\right]^2+\frac{(1-\left(\frac{\tau c}{D}\right)^2)\frac{1-x^2}{1+x^2}}{\frac{1-x^2}{1+x^2}-\frac{\tau c}{D}}\right\}$$

The last step above uses these coordinate transformation identities $x = \tan\frac{\theta_u}{2}$, $\sin\theta_u = \frac{2x}{x^2+1}$, $\cos\theta_u = \frac{1-x^2}{1+x^2}$, $d\theta_u = \frac{2dx}{x^2+1}$, and $x^2 = \frac{1-\cos\theta_u}{1+\cos\theta_u}$, which give:

$x_1 = \sqrt{\frac{(\frac{R}{D})^2-(1-\frac{\tau c}{D}+\frac{R}{D})^2}{(1+\frac{\tau c}{D}-\frac{R}{D})^2-(\frac{R}{D})^2}}$ Substituting $x = 0$ in the primitive gives 0; hence, the integral

needs to be evaluated only at x_1. All these imply that for $\tau \in \left(\frac{D}{c}, \frac{D+2R}{c}\right)$,

$$\begin{aligned} f_\tau(\tau) = \quad & \frac{c/D}{96S_2\pi(1-\frac{\tau c}{D})}\left(\frac{R}{D}\right)^{-4}\Bigg\{48\frac{R}{D}\left(\frac{\tau c}{D}\right)^3 S_1S_2 - 18\frac{\tau c}{D}S_3 \\ & +23S_1S_2\frac{\tau c}{D} - 28\frac{R}{D}\frac{\tau c}{D}S_1S_2 + 192\left(\frac{R}{D}\right)^2\left(\frac{\tau c}{D}\right)^2 S_3 \\ & +23\left(\frac{\tau c}{D}\right)^2 S_1S_2 + 48\left(\frac{\tau c}{D}\right)^5 S_3 - 36\left(\frac{R}{D}\right)^2 S_1S_2 \\ & -128\left(\frac{R}{D}\right)^3\frac{\tau c}{D}S_1S_2 - 192\left(\frac{R}{D}\right)^2\left(\frac{\tau c}{D}\right)^3 S_3 \\ & +96\left(\frac{R}{D}\right)^4 S_1S_2 - 28\frac{R}{D}\left(\frac{\tau c}{D}\right)^2 S_1S_2 - 96\left(\frac{R}{D}\right)^2 S_3 \\ & -38\left(\frac{\tau c}{D}\right)^4 S_1S_2 - 48\left(\frac{R}{D}\right)^3 S_1S_2 - 38\left(\frac{\tau c}{D}\right)^3 S_1S_2 \\ & +18S_3 + 96\left(\frac{R}{D}\right)^2\left(\frac{\tau c}{D}\right)^2 S_1S_2 + 40\left(\frac{R}{D}\right)^2\frac{\tau c}{D}S_1S_2 \\ & +18S_1S_2\frac{R}{D} - 48\left(\frac{\tau c}{D}\right)^4 S_3 + 96\frac{\tau c}{D}\left(\frac{R}{D}\right)^2 S_3\Bigg\} \end{aligned} \tag{3.4}$$

with $S_0 = \frac{\tau c}{D} + 1$, $S_1 = \sqrt{\frac{-\left[1-2\frac{\tau c}{D}+2\frac{R}{D}+(\frac{\tau c}{D})^2-2\frac{\tau c}{D}\frac{R}{D}\right]}{\left[1+2\frac{\tau c}{D}-2\frac{R}{D}+(\frac{\tau c}{D})^2-2\frac{\tau c}{D}\frac{R}{D}\right]}}$, $S_2 = \sqrt{\left(\frac{\tau c}{D}-1\right)\left(\frac{\tau c}{D}+1\right)}$, and $S_3 = \arctan\left(\frac{S_0S_1}{S_2}\right)$.

3.6 Downlink's Multipaths' TOA-AOA Distributions

The scatterers' spatial symmetry around the mobile implies that multipaths' AOA density at the mobile to equal $f_{\theta_d}(\theta_d) = \frac{1}{2\pi}$, for $\theta_d \in [-\pi, \pi)$.

The travelled distance of each multipath from the base station to the mobile station is independent of the propagations direction. Therefore, the TOA propagation delay's distribution remains to be $f_\tau(\tau)$.

The TOA-AOA joint distribution may be non-zero only for $\frac{1-(\frac{\tau c}{D})^2}{2\left(\cos(\theta_d)-\frac{\tau c}{D}\right)} \le \frac{R}{D}$, whereby $r_s = \frac{D^2-\tau^2c^2}{2(D\cos(\theta_d)-\tau c)}$ and thus $f_{x,y}\left(r_s\cos(\theta_d)+D, r_s\sin(\theta_d)\right) = \frac{2}{\pi R^4}\left\{R^2 - \left[\frac{D^2-\tau^2c^2}{2(D\cos(\theta_d)-\tau c)}\right]^2\right\}$,

giving $f_{\tau,\theta_d}(\tau,\theta_d) =$

$$= \left\{ \frac{\left[1-\left(\frac{\tau c}{D}\right)^2\right]\left[1+\left(\frac{\tau c}{D}\right)^2-2\frac{\tau c}{D}\cos(\theta_d)\right]}{\left[\cos(\theta_d)-\frac{\tau c}{D}\right]^3} \right\}$$
$$\frac{c}{2\pi D}\left(\frac{R}{D}\right)^{-4}\left\{\left(\frac{R}{D}\right)^2-\left[\frac{1-\left(\frac{\tau c}{D}\right)^2}{2\left(\cos(\theta_d)-\frac{\tau c}{D}\right)}\right]^2\right\}$$

Otherwise, $f_{\tau,\theta_d}(\tau,\theta_d) = 0$. Figure 3.4 plots $f_{\tau,\theta_d}(\tau,\theta_d)$ for $R = 100$ meters and $D = 1000$ meters.

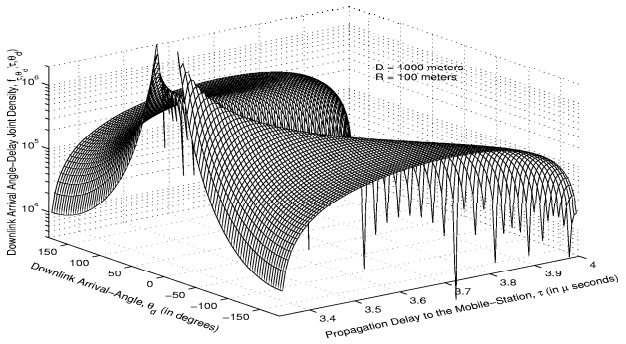

Figure 3.4: $f_{\tau,\theta_d}(\tau,\theta_d)$, at $R = 100$ meters and $D = 1000$ meters.

Chapter 4

Compare and Contrast of Geometric Models

It would be of interest to calibrate the independent variables of geometric analytical models using empirically measured data. To this date, such laborious tasks have not been adequately performed in a systemic manner. With these calibrations, we can then classify which models are best suited for a particular enviroment. For example, downtown urban areas with high-rises exhibit similar wireless channel statistics whether it be downtown Tokyo or downtown Toronto. Suburban areas with relatively flat human-made structures (i.e., buildings not more than a few floors high) exhibit another type of channel statistics. Mountainous areas in Switzerland or the Rockies, for example, fall into another class of their own. Spread out throughout the research literature are many such empirical studies, but they have been inadequately compared and systematized.

The papers [3], [5], [7], [8], [10], [15], [17], [20], [21], [23], [24], [25], have rigorously derived closed-form geometric models to represent an abstract wireless environment. These papers will be compared with empirical measurements to help classify which geometric

models are best suited for a particular environment.

When deriving the geometric model, the author does not explicitly state all the possible assumptions pertaining to the model being derived. As a result, there are many assumptions that are omitted in the paper which should have been included. Both explicit and implicit assumptions must be stated in order to have an accurate model. Any assumptions not stated in the paper but implied in the derivation of the geometric model have been added. The following table contains both implicit and explicit assumptions of these geometric models.

The table also contains the mathematical expressions for DOA marginal distribution, TOA marginal distribution, and joint DOA-TOA distribution. The DOA marginal is then plotted in Figure 4. The geometric model parameters used in Table 1 and here on in are defined as follows:

θ - The angle of arrival of the planar wave from MS or BS.

R - The radius of the circular disc of scatterers surrounding the MS.

D - The distance between the MS and the BS.

σ - The standard deviation of scatterers around MS.

r - The inner radius of the hollow circular disc of scatterers around MS.

τ_m - The maximum delay for a mulitpath signal.

Reference	Scatterer Spatial Distribution	$f_\theta(\theta)$	$f_\tau(\tau)$	$f_{\theta,\tau}(\theta,\tau)$
Lee	Uniform, circular ring around MS	see [8]	not derived	not derived
VanRheedenICCC98	Uniform on circular disc around MS	$\frac{2}{\pi}\frac{D}{R}\cos\theta\sqrt{1-(\frac{D}{R})^2\sin^2\theta},\ \theta\in\left[-\arcsin\frac{R}{D},\arcsin\frac{R}{D}\right]$	not derived	not derived
EggersEL0198	Uniform on circular disc around MS	$\frac{2}{\pi}\frac{D}{R}\cos\theta\sqrt{1-(\frac{D}{R})^2\sin^2\theta}$	not derived	not derived
PiechockiEL0998	Uniform on circular disc around MS	$\frac{2}{\pi}\frac{D}{R}\cos\theta\sqrt{1-(\frac{D}{R})^2\sin^2\theta}$	not derived	not derived
ErtelJSAC1199	Uniform on circular disc around MS	$\frac{2}{\pi}\frac{D}{R}\cos\theta\sqrt{1-(\frac{D}{R})^2\sin^2\theta}$	see Equation (4.1)	see Equation (4.2)
PetrusCT0302[1] PetrusCL0397	Uniform on circular disc around MS	$\frac{2}{\pi}\frac{D}{R}\cos\theta\sqrt{1-(\frac{D}{R})^2\sin^2\theta}$	not derived	not derived
EggersEL0198	Conical on circular disc around MS	see Equation (4.3)	not derived	not derived
LotterCL05999[2]	Gaussian around MS	$\frac{1}{2\sqrt{2\pi}\sigma}e^{\frac{D^2(\cos^2\theta-1)}{2\sigma^2}}erfc(\frac{-D\cos\theta}{\sqrt{2}\sigma})$	not derived	not derived
JanaswamyWCT0702[3]	Gaussian around MS	$\frac{1}{2\pi}e^{\frac{-D^2}{2\sigma^2}}+\frac{D\cos\theta}{2\sqrt{2\pi}\sigma}e^{\frac{D^2(\cos^2\theta-1)}{2\sigma^2}}erfc(\frac{-D\cos\theta}{\sqrt{2}\sigma})$	not in closed form, see Equation (4.6)	not derived
LaurilaISSTA98[4]	Rayleigh around MS	see Equation (4.4)	not in closed form, see Equation (4.5)	not derived
JanaswamyVTT0902	Uniform, 3D Spheroid around MS	Azimuth: $\frac{3D}{4R}\cos\theta(1-(\frac{D}{R})^2\sin^2\theta)$ Elevation: not closed form, see [23], eq. (35)	not derived	not derived
OlenkoWongAbdulla	Inverted Parabolic around MS	$\frac{8D^4cos\theta}{3\pi R^4}\left((\frac{R}{D})^2-sin^2\theta\right)^{\frac{3}{2}}$	see [25], eq (4)	see [25]
OlenkoAWPL03	Uniform on hollow disc around MS	$\frac{2\cos\theta}{\pi}\frac{\sqrt{(\frac{R}{D})^2-\sin^2\theta}-\sqrt{(\frac{r}{D})^2-\sin^2\theta}}{(\frac{R}{D})^2-(\frac{r}{D})^2},\ \theta\in\left[0,\arcsin\frac{r}{D}\right.$ $\frac{2cos\theta}{\pi}\frac{\sqrt{(\frac{R}{D})^2-sin^2\theta}}{(\frac{R}{D})^2-(\frac{r}{D})^2},\ \theta\in\left[-\arcsin\frac{R}{D},\arcsin\frac{R}{D}\right]$	see [24], eq (9)	see [24], eq (3)
ErtelJSAC1199	Uniform on elliptical disc around MS and BS	$\frac{1}{8a_mb_m}\left(\frac{\tau_m^2c^2-D^2}{\tau_mc-D\cos\theta}\right)^2\ a_m=\frac{c\tau_m}{2},b_m=\frac{1}{2}\sqrt{c^2\tau^2-D^2}$	see Equation (4.8)	see Equation (4.7)
Liberti1VTC96	Uniform on elliptical rim around MS and BS	$\frac{2r-1}{r_m\sqrt{r_m^2-1}\sqrt{r^2-1}},r=\tau c/D,r_m=\tau_mc/D$	not derived	not derived

Table 4.1: Probability density functions for "Geometrical Models"

[1]Unless otherwise stated, the model 1) each propagation path has only a single bounce off one scatterer, 2) excludes the LOS path from the transmitter to the receiver, 3) ignores polarization effects, 4) ignores elevation angle, 5) assumes all antennas as omni-directional, and 6) with all scatterers as isotropic lossless re-transmitters.

[2]This paper has also derived the downlink AOA distributions

[3]The DOA model with a Gaussian distribution of scatterers around the MS presented in LotterCL0599,[15], does not approach uniform distribution when $D/\sigma = 0$. Instead it approaches zero which is clearly incorrect. As a result, this model is omitted in the empirical comparison. The correct Gaussian model derived in JanaswamyWCT0702 is used instead. Any reference herein to the gaussian model is associated with this model.

[4]This paper has also derived the downlink AOA distributions

Due to space limitations, the following are equations referred in Table 1.

$$f_\tau(\tau) = \frac{c}{\pi D}\left(\frac{R}{D}\right)^{-2}\left\{\frac{\pi\left(\frac{\tau c}{D}\right)^2 k_2 - \frac{\tau c}{D}k_1^2 + \pi k_2 k_1^2 + \frac{\tau c}{D}k_1^2 - 2\frac{R}{D}k_1^2}{4k_1k_2} + \frac{\left(\frac{\tau c}{D}\right)^2 k_0k_4 + \frac{\tau c}{D}k_0k_1^2}{2k_4^2 + 2k_0^2k_1^2}\right.$$
$$\left. + \frac{\left(\frac{\tau c}{D}\right)^2 + k_1^2}{2k_1}\arctan\left(\frac{k_0k_1}{k_4}\right) - \frac{\frac{R}{D} - \frac{\tau c}{D}}{\sqrt{4\left(\frac{R}{D}\right)^2 - k_3^2}}\left(2\left(\frac{R}{D}\right)^2 + \frac{\frac{\tau c}{D}k_1^2k_4(1+k_0^2)}{2k_4^2 + 2k_0^2k_1^2}\right)\right\} \quad (4.1)$$

where

$$k_0 = \tan\left(\frac{1}{2}\arccos\left[\frac{-\left(\frac{\tau c}{D}\right)^2 + 1 + 2\frac{R}{D}\frac{\tau c}{D}}{2\frac{R}{D}}\right]\right)$$

$$k_1 = \sqrt{\left(\frac{\tau c}{D}\right)^2 - 1}$$

$$k_2 = \sqrt{1 - 4\left(\frac{R}{D}\right)^2 - \left(\frac{\tau c}{D}\right)^2 + 4\frac{R}{D}\frac{\tau c}{D}}$$

$$k_3 = -\left(\frac{\tau c}{D}\right)^2 + 1 + 2\frac{R}{D}\frac{\tau c}{D}$$

$$k_4 = 1 - \frac{\tau c}{D}$$

$$f_{\theta,\tau}(\theta,\tau) = \begin{cases} \frac{\left(D^2+\tau^2c^2\right)\left(D^2c+\tau^2c^3-2\tau c^2D\cos\theta\right)}{4\pi R^4(Dcos\theta-\tau c)^3}, & \frac{D^2-2\tau cD\cos\theta+\tau^2c^2}{\tau c-D\cos\theta} \leq 2R \\ \frac{c(D+\tau c)}{4\pi R^2}, & \frac{D}{c} \leq \tau \leq \frac{D+2R}{c}, \theta = 0 \end{cases} \quad (4.2)$$

[5]The Rayleigh scatterer distribution around the MS, proposed and derived in the paper LaurilaISSTA98 assumes $D >> R$. For D/R, not large, the distribution could become negative. Secondly, when $D/R >> 1$, the Rayliegh-distributed scatterers' $f_\theta(\theta)$ approaches the Gaussian distributed scatterers' $f_\theta(\theta)$. Hence, this model is omitted in the empirical comparison. A detailed comparison between the rayleigh and gaussian distribution of scatterers is found in the Appendix.

$$f_\theta(\theta) = \begin{cases} \frac{3\Gamma\sin\theta}{2\pi}\left\{2\Psi - \Gamma^2\cos^2\theta\ln\left(\frac{1+\Psi}{1-\Psi}\right)\right\}, & \Gamma \geq 1 \\ \frac{3}{2\pi}\left\{\frac{1}{3} + \frac{2}{3}\Gamma^3 + \Gamma\sin\theta\left[(2\Gamma - \Gamma^2)\sin\theta + \Psi - \Gamma^2\cos^2\theta\ln\left(\frac{1+\Psi}{\Gamma - \Gamma\sin\theta}\right)\right]\right\}, & \Gamma < 1 \end{cases} \quad (4.3)$$

where

$$\Gamma = \frac{D}{R}$$

$$\Psi = \sqrt{1 - \Gamma^2\cos^2\theta}$$

$$\theta \in \left[-\arcsin\left(\frac{1}{\Gamma}\right), \arcsin\left(\frac{1}{\Gamma}\right)\right]$$

$$f_\theta(\theta) = \frac{1}{2\pi}e^{-\frac{D^2}{2R^2}}\left\{1 + erf\left(\frac{D\cos\theta}{\sqrt{2}R}\right)\right\}\left\{1 + \sqrt{\frac{\pi}{2}}\frac{D}{R}\cos\theta e^{\frac{D^2\cos^2\theta}{2R^2}}\right\}, \theta \in [-\pi, \pi] \quad (4.4)$$

$$f_\tau(\tau) = \int_0^\pi \frac{cv\left(D^2 - c^2\tau^2\right)}{8\pi^2\tau^2\left(D\cos u - c\tau\right)^2} exp\left(-\frac{\left(D^2 - c\tau\right)^2 - 4vDc\tau\cos u}{8R^2\left(D\cos u - c\tau\right)^2}\right) du \quad (4.5)$$

where

$$v = D^2 + c^2\tau^2 - Dc\tau\cos u$$

$$f_\tau(\tau) = \frac{1}{2\pi\tau_o}D_s^2\frac{exp\left(-D_s^2\tau_n/8\right)}{\sqrt{(}\tau_n^2 - 1}\int_0^{\pi/2}\left(\tau_n^2 - \sin^2\theta\right)exp\left(-D_s^2\sin^2\theta/8\right)cosh\left(\frac{\tau_n^2 D_s^2\sin\theta}{4}\right)d\theta \quad (4.6)$$

where $\tau_o = \frac{D}{c}$, $\tau_n = \frac{\tau}{\tau_o}$, $D_s = \frac{D}{\sigma}$

$$f_{\theta,\tau}(\theta,\tau) = \frac{\left(D^2 - \tau^2c^2\right)\left(D^2c + \tau^2c^3 - 2\tau c^2 D\cos\theta\right)}{4\pi a_m b_m\left(D\cos\theta - \tau c\right)^3} \quad (4.7)$$

$$f_\tau(\tau) = \frac{c\left(2\tau^2c^2 - D^2\right)}{4\pi a_m b_m\sqrt{\tau^2c^2 - D^2}} \quad (4.8)$$

where in both above equations, $a_m = \frac{c\tau_m}{2}$ and $b_m = \frac{1}{2}\sqrt{c^2\tau^2 - D^2}$

$$
\begin{aligned}
f_{\tau,\theta}(\tau,\theta) &= \frac{c}{2\pi D}\left(\frac{R}{D}\right)^{-4}\frac{\left[1-\left(\frac{\tau c}{D}\right)^2\right]\left[1+\left(\frac{\tau c}{D}\right)^2-2\frac{\tau c}{D}\cos\theta\right]}{\left(\cos\theta-\frac{\tau c}{D}\right)^3} \\
&\quad \left\{\left(\frac{R}{D}\right)^2 - 1 - \left[\frac{1-(\frac{\tau c}{D})^2}{2(\cos\theta-\frac{\tau c}{D})}\right]^2 + \frac{\left[1-\left(\frac{\tau c}{D}\right)^2\right]\cos\theta}{\cos\theta-\frac{\tau c}{D}}\right\} \qquad (4.9)
\end{aligned}
$$

$$
\begin{aligned}
f_{\tau}(\tau) &= \frac{c/D}{96S_2\pi(1-\frac{\tau c}{D})}\left(\frac{R}{D}\right)^{-4}\left\{48\frac{R}{D}\left(\frac{\tau c}{D}\right)^3 S_1S_2 - 18\frac{\tau c}{D}S_3 + 23S_1S_2\frac{\tau c}{D} - 28\frac{R}{D}\frac{\tau c}{D}S_1S_2\right. \\
&\quad +192\left(\frac{R}{D}\right)^2\left(\frac{\tau c}{D}\right)^2 S_3 + 23\left(\frac{\tau c}{D}\right)^2 S_1S_2 + 48\left(\frac{\tau c}{D}\right)^5 S_3 - 36\left(\frac{R}{D}\right)^2 S_1S_2 + 18S_1S_2\frac{R}{D} \\
&\quad -128\left(\frac{R}{D}\right)^3\frac{\tau c}{D}S_1S_2 - 192\left(\frac{R}{D}\right)^2\left(\frac{\tau c}{D}\right)^3 S_3 + 96\left(\frac{R}{D}\right)^4 S_1S_2 - 28\frac{R}{D}\left(\frac{\tau c}{D}\right)^2 S_1S_2 \\
&\quad -96\left(\frac{R}{D}\right)^2 S_3 - 38\left(\frac{\tau c}{D}\right)^4 S_1S_2 - 48\left(\frac{R}{D}\right)^3 S_1S_2 - 38\left(\frac{\tau c}{D}\right)^3 S_1S_2 + 18S_3 \\
&\quad \left.+96\left(\frac{R}{D}\right)^2\left(\frac{\tau c}{D}\right)^2 S_1S_2 + 40\left(\frac{R}{D}\right)^2\frac{\tau c}{D}S_1S_2 - 48\left(\frac{\tau c}{D}\right)^4 S_3 + 96\frac{\tau c}{D}\left(\frac{R}{D}\right)^2 S_3\right\} \qquad (4.10)
\end{aligned}
$$

where

$$
\begin{aligned}
S_0 &= \tfrac{\tau c}{D} + 1, \\
S_1 &= \sqrt{\frac{-\left[1-2\frac{\tau c}{D}+2\frac{R}{D}+(\frac{\tau c}{D})^2-2\frac{\tau c}{D}\frac{R}{D}\right]}{\left[1+2\frac{\tau c}{D}-2\frac{R}{D}+(\frac{\tau c}{D})^2-2\frac{\tau c}{D}\frac{R}{D}\right]}}, \\
S_2 &= \sqrt{\left(\tfrac{\tau c}{D}-1\right)\left(\tfrac{\tau c}{D}+1\right)}, \\
S_3 &= \arctan\left(\tfrac{S_0S_1}{S_2}\right).
\end{aligned}
$$

$$
f_{\tau,\theta}(\tau,\theta) = \frac{c}{4\pi D}\frac{1-\left(\frac{\tau c}{D}\right)^2}{\left(\frac{R}{D}\right)^2-\left(\frac{r}{D}\right)^2}\frac{1+\left(\frac{\tau c}{D}\right)^2-2\frac{\tau c}{D}\cos\theta}{\left(\cos\theta-\frac{\tau c}{D}\right)^3} \qquad (4.11)
$$

$$
f_\tau(\tau) = \begin{cases} = \frac{-c\left(\frac{R}{D}-\frac{c\tau}{D}\right)^2[S_{11}S_{12}S_{13}+S_{14}(S_{15}+S_{16})]}{2\pi D\left[\left(\frac{r}{D}\right)^2-\left(\frac{R}{D}\right)^2\right]\left[\frac{c\tau}{D}-\frac{R}{D}\right]\left[\left(\frac{c\tau}{D}\right)^2-1\right]^{5/2}}, & \text{if } \tau \in \left[\frac{D+2r}{c}, \frac{D+2R}{c}\right] \\ = S_{21}\left\{S_{22}\left[S_{24}-S_{23}\right]+S_{25}\left[S_{26}S_{27}^3S_{28}+\left(1-\frac{c\tau}{D}\right)\right.\right. & \\ \left[S_{36}\left(S_{29}-S_{30}\right)-4S_{29}S_{31}^2\left(1-\frac{c\tau}{D}-S_{31}^2\right)-8S_{31}^3S_{32}\right]+4S_{27}^2 & \\ \left.\left.\left(S_{30}+S_{33}\right)\left(1-\frac{c\tau}{D}-S_{27}^2\right)\right]\right\}, & \text{if } \tau \in \left[\frac{D}{c}, \frac{D+2r}{c}\right] \\ 0, & \text{otherwise} \end{cases} \tag{4.12}
$$

where

$$
\begin{aligned}
S_{11} &= 2\left[1-2\left(\frac{c\tau}{D}\right)^2\right] \\
S_{12} &= \arctan\left[\frac{\left(1+\frac{c\tau}{D}\right)\cot\left[\frac{1}{2}S_{17}\right]}{\sqrt{\left(\frac{c\tau}{D}\right)^2-1}}\right] \\
S_{13} &= -2\left(\frac{c\tau}{D}\right)^2\left(\frac{R}{D}\right)+\frac{R}{D}+\frac{c\tau}{D}+ \\
&\quad \left(\frac{R}{D}-\frac{c\tau}{D}\right)\cos\left[2S_{17}\right] \\
S_{14} &= \left(\frac{c\tau}{D}-\frac{R}{D}\right)\sqrt{\left(\frac{c\tau}{D}\right)^2-1} \\
S_{15} &= \sqrt{\frac{\left[\left(\frac{c\tau}{D}\right)^2-1\right]\left[1-\left(\frac{c\tau}{D}-2\frac{R}{D}\right)^2\right]}{\left(\frac{R}{D}-\frac{c\tau}{D}\right)^2}} \\
S_{16} &= \frac{c\tau}{D}\sin\left[2S_{17}\right] \\
S_{17} &= \arccos\left[\frac{1-2\frac{R}{D}\frac{c\tau}{D}+\left(\frac{c\tau}{D}\right)^2}{2\frac{R}{D}-2\frac{c\tau}{D}}\right] \\
S_{21} &= \frac{c\left(\frac{r}{D}-\frac{c\tau}{D}\right)^2\left(\frac{R}{D}-\frac{c\tau}{D}\right)^2}{2\pi D\left[\left(\frac{r}{D}\right)^2-\left(\frac{R}{D}\right)^2\right]\left[\left(\frac{c\tau}{D}\right)^2-1\right]^{9/2}} \\
S_{22} &= \frac{\left[1-2\left(\frac{c\tau}{D}\right)^2\right]\left[1-\left(\frac{c\tau}{D}\right)^2\right]^4}{\left(\frac{r}{D}-\frac{c\tau}{D}\right)^2\left(\frac{R}{D}-\frac{c\tau}{D}\right)^2} \\
S_{23} &= \arctan\left[\frac{\left(1+\frac{c\tau}{D}\right)\cot\left[\frac{1}{2}S_{35}\right]}{\sqrt{\left(\frac{c\tau}{D}\right)^2-1}}\right] \\
S_{24} &= \arctan\left[\frac{\left(1+\frac{c\tau}{D}\right)\cot\left[\frac{1}{2}S_{34}\right]}{\sqrt{\left(\frac{c\tau}{D}\right)^2-1}}\right] \\
S_{25} &= 4\sqrt{\left(\frac{c\tau}{D}\right)^2-1}
\end{aligned}
$$

$$
\begin{aligned}
S_{26} &= \frac{2\frac{c\tau}{D}\left[1-\left(\frac{c\tau}{D}\right)^2\right]^2}{\left(\frac{R}{D}-\frac{c\tau}{D}\right)^2} \\
S_{27} &= \cos\left[\frac{1}{2}S_{35}\right]; \quad S_{28} = \sin\left[\frac{1}{2}S_{35}\right] \\
S_{29} &= \sqrt{\frac{\left[\left(\frac{c\tau}{D}\right)^2-1\right]\left[1-\left(\frac{c\tau}{D}-2\frac{r}{D}\right)^2\right]}{\left(\frac{r}{D}-\frac{c\tau}{D}\right)^2}} \\
S_{30} &= \sqrt{\frac{\left[\left(\frac{c\tau}{D}\right)^2-1\right]\left[1-\left(\frac{c\tau}{D}-2\frac{R}{D}\right)^2\right]}{\left(\frac{R}{D}-\frac{c\tau}{D}\right)^2}} \\
S_{31} &= \cos\left(\frac{1}{2}S_{34}\right); \\
S_{32} &= \sin\left(\frac{1}{2}S_{34}\right)\left[\frac{c\tau}{D}-\left(\frac{c\tau}{D}\right)^2\right] \\
S_{33} &= \frac{c\tau}{D}\sin\left(2S_{34}\right) \\
S_{34} &= \arccos\left(\frac{1-2\frac{R}{D}\frac{c\tau}{D}+\left(\frac{c\tau}{D}\right)^2}{2\frac{R}{D}-2\frac{c\tau}{D}}\right) \\
S_{35} &= \arccos\left(\frac{1-2\frac{r}{D}\frac{c\tau}{D}+\left(\frac{c\tau}{D}\right)^2}{2\frac{r}{D}-2\frac{c\tau}{D}}\right) \\
S_{36} &= 1-2\frac{c\tau}{D}+\left(\frac{c\tau}{D}\right)^2
\end{aligned}
$$

Various geometric model's $f_\theta(\theta)$ are plotted in Figure 4. Analysis on TOA distribution data is beyond the scope of this research and some results can be found in the appendix.

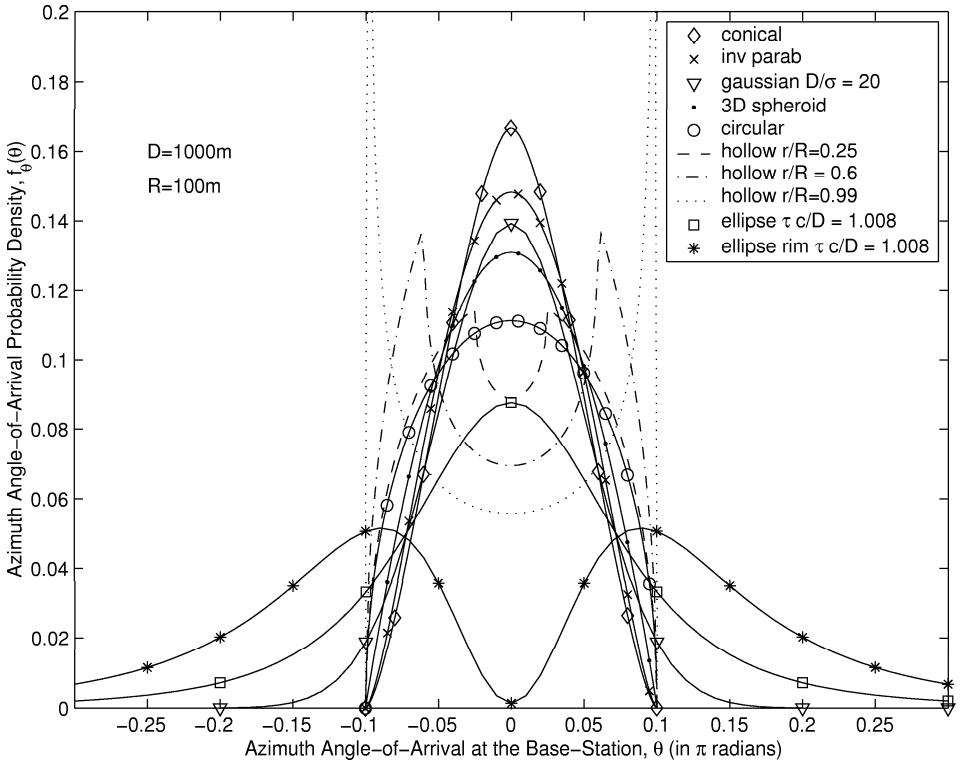

Figure 4.1: AOA distribution for all geometric models

AOA marginal distribution curves use multiple parameters which characterize the shape of the curve. These parameters are defined and described below:

1) D/R: This parameter determines the maximum and minimum values of the angle of arrival, θ, where $\theta\epsilon\left[-\arcsin\left(\frac{R}{D}\right), \arcsin\left(\frac{R}{D}\right)\right]$. As D/R increases, the theoretical $f_\theta(\theta)$, decreases in width and increses in height. As $D/R \to \infty$, $f_\theta(\theta) \to \delta(\theta)$, an impluse function. If $D/R < 1$, the base stations lies inside the region of scatterers.

As a result, the plane waves will arrive at an angle greater than 90 degrees from the LOS. When $D/R \rightarrow 0$, $f_\theta(\theta)$ becomes 'flatter' with respect to θ and $f_\theta(\theta) = \frac{1}{2\pi}, \forall\theta$, a uniform distribution.

$$f_\theta(\theta) \rightarrow \begin{cases} \delta(\theta) \ \ \forall\theta, & as \ \ \frac{D}{R} \rightarrow \infty \\ \frac{1}{2\pi} \ \ \forall\theta, & as \ \ \frac{D}{R} \rightarrow 0 \end{cases}$$

It is to be noted that not all geometric models that use this parameter have a close form derivation when $D/R < 1$. Only the conical and circular uniform scatterer distribution models derive an expression to satisfy this condition. The inverted parabolic, 3D uniform spheroid, and the hollow disc geometric models do not such a condition. In these model derivations, D/R can only be ≥ 1.

2) D/σ: This parameter is used in the Gaussian scatterer distribution model. As D/σ increases, the distance between the BS and MS increases and $f_\theta(\theta)$ becomes narrower with respect to θ. When $D/\sigma \rightarrow \infty$, $f_\theta(\theta) \rightarrow \delta$. On the other hand, if this ratio decreases below unity, the BS lies inside the region of scatterers and thus the angle can arrive from all possible directions.

$$f_\theta(\theta) \rightarrow \begin{cases} \delta(\theta) \ \ \forall\theta, & as \ \ \frac{D}{\sigma} \rightarrow \infty \\ \frac{1}{2\pi} \ \ \forall\theta, & as \ \ \frac{D}{\sigma} \rightarrow 0 \end{cases}$$

3) r/R: This parameter is used only in the hollow disc scatterer distribution model. When $r/R \rightarrow 0$, we obtain a circular disc of scatteres and the DOA curve reduces to the uniform scatterer distribution model. When $r/R \rightarrow 1$, the inner and outer length of the hollow disc are equal and we obtain the circular ring of scatterers distribution model.

4) $\tau_m c/D$: This parameter is used only in the elliptical and elliptical rim scatterer distribution model. In these model derivations, $\tau_m c/D > 1$. As $\tau_m c/D$ increases, we essentially increase the maximum delay with repect to the seperation between the MS and BS. As a result, we are increasing the minor axis of the ellipse. This results in the AOA distribution having a uniform distribution. As $\tau_m c/D$ approaches 1, we decrease the minor axis and increase the major axis resulting in an impulse function.

$$f_\theta(\theta) \rightarrow \begin{cases} \delta(\theta) \ \ \forall\theta, & as \ \ \frac{\tau_m c}{D} \rightarrow 1 \\ \frac{1}{2\pi} \ \ \forall\theta, & as \ \ \frac{\tau_m c}{D} \rightarrow \infty \end{cases}$$

azimuth angles) around the mobile:

Table 4.2 summarizes the angle of arrival distribution curve as each parameter is varied.

Parameter	$\rightarrow 0$	$\rightarrow \infty$	$\rightarrow 1$	Geometry of Model
D/R	uniform distribution	$\delta(\theta)$	N/A	uniform on circular disc, conical on circular disc, uniform on hollow disc, inverted parabolic
D/σ	uniform distribution	$\delta(\theta)$	N/A	gaussian model
r/R	uniform on circular disc	N/A	uniform circular ring	unifrom on hollow disc
$\tau c/D$	NA	$\delta(\theta)$	uniform distribution	uniform on ellipse uniform on ellipse rim

Table 4.2: Summary of DOA distribution curve parameters

The parameters discussed above also affect other features of AOA curves as follows:

1) Unimodal vs Multi-modal - AOA distribution curves seen in Figure 4 are either unimodal or multi-modal. A unimodal distribution occurs in all geometric models that have scattereres distributed with a circular region surrounding the mobile. A multi-modal distribution can only be seen in the geometric model where the scatterers are distributed in a hollow disc surrounding the mobile. The two peaks of this multi-model distribution depends on the parameter value, r/R. As r/R increases, the height of each peak also increases. The peaks reach a maximum height as r/R approaches 1, the circular ring of scatterers model. A multi-modal distribution also occurs for the elliptical rim scatterer distribution model. By decreasing the parameter value $\tau_m c/D$ we essentially increase the BS and MS seperation w.r.t the maximum path delay. As a result, the peak increases in height.

2) Width of main peak - The width of the main peak depends on distribution of scatteres. For geometric models that use the parameter D/R, the width of the AOA curve is defined to be $2\arcsin(R/D)$ radians. For geometric models that have scatterer distributions that does not end outside a predetermined radius value but intead which continue to infinity and/or in which the BS is enclosed within the scatterer distribution, such as the gaussian and/or the elliptical distribution models, the recieved signal at the BS comes from all possible angles. Therefore, the width of the AOA curve is the entire angle space region defined as 2π radians.

3) Finite AOA spread - The AOA spread for all geometric models can be calculated using the following formula.

$$s = \sqrt{E[\theta_b^2] - E[\theta_b]^2} \tag{4.13}$$

The angular spread is a statistic that measures the dispersiveness of the wireless

channel. In another words, it is the standard deviation of the angle of arrival seen at the base station.

Symbolic mathematic programming could find a closed-form solution for any of the geometric models except the 3D spherical model. The AOA spread for this model is shown in Equation 4.14. To determine the AOA spread for all other models, numerical integration must be used.

$$s_{3D} = \frac{1}{9}\left\{6\Gamma^2 - 26 - 6\Gamma\left(\Gamma^2 - 4\right)\sqrt{1 - \frac{1}{\Gamma^2}}\arcsin\left(\frac{1}{\Gamma}\right) + 9\arcsin^2\left(\frac{1}{\Gamma}\right)\right\} \quad (4.14)$$

Chapter 5

Compare and Contrast of Empirical Data

Empirical measurements have been taken in different outdoor propagation environments. Due to the scope of this research, outdoor channel sounding measurements are not performed by the author. Instead, empirical measurements published in various conferences and journals are extracted and use for comparison. In order to compare empirical measurements accurately, the empirical data is first used to generate model parameters (described in the previous section) such as distance between mobile and base station, D, radius of scatterer distributions, R, standard deviation of scatterer density, σ, etc.

5.1 Least-Square-Error Fitting of AOA models

To compare and contrast various geometric model's closeness to reality, each geometrical model in Table 1 is calibrated by each set of empirical fading dataset in Table 3. The least-square-error (LSE) between each pair of geometric model and empirical data indications the

goodness of the fit between the two. Both the geometric model and the empirical dataset are each normalized to give a distribution that sume to one, then the LSE is computed as follows:

$$LSE \quad = \quad \frac{1}{N}\sum_{n=1}^{N} d_n^2 \quad = \quad \frac{1}{N}\sum_{n=1}^{N} [y_n - f(x_n)]^2 \tag{5.1}$$

where:

d_n = least-square-fit error for the n-th point

x_n = the n-th grid point along the θ-coordinate or τ-coordinate

y_n = the empirical signal's normalized strength at $\theta = x_n$ or $\tau = x_n$

$f(x_n)$ = the geometric model's prediction

Based on this LSE formula, we can use an empirical dataset E_m to calibrate a geometric model, G_n, to determine its independent parameter that results in the best fit. For all empirical datasets, $(E_1, E_2, ..., E_M)$, and all geometric models, $(G_1, G_2, ..., G_N)$, we can formulate MN least-square errors. In order to properly compare and constrast the LSE values among each other, we must also normalize the LSE values. The LSE values have been normalized by the number of datapoints, N.

For papers where the probability density function is not explicity stated, but instead the power of each individual multipaths, the cumulative distribution function is calculated for each given empirical dataset. The cumulative distribution function is also generated for the theoretical model. The LSE is then calculated by using both these cumulative distribution functions.

The LSE values for all AOA models discussed thus far and empirical datasets are shown in Table 5.1, various papers' empirical data have been plotted against the calibrated geometric models and are found in Figures 5.1a to 5.4c.

Reference	Env	Circular Disc		Hollow Disc		Conical		Inv. Parab		Gaussian		Ellipse		Ellipse Rim		3D spheroid	
		LSE	D/R	LSE	D/R	LSE	D/σ	LSE	D/R	LSE	D/R	LSE	r/R D/R	LSE	$\tau c/D$	LSE	$\tau c/D$
KleinISSTA96 1	R	0.140	3.82	0.140	3.82	0.087	2.88	0.102	3.11	0.071	6.96	0.041	1.0240	0.309	1.0053	0.114	3.46
MatthewsICMPRC89 1	R	0.0091	4.12	0.0092	4.12	0.0028	2.97	0.0033	3.24	0.0023	7.07	0.0059	1.0248	0.1128	1.0059	0.0053	3.68
MatthewsICMPRC89 2	R	0.028	0.80	0.030	1	0.025	0.61	0.034	1.00	0.027	1.10	0.022	1.3430	0.0386	1.536	0.032	1.00
PedersenVTC98	R	18.1	35.77	18.3	35.71	11.0	24.83	13.5	25.96	9.4	59.73	5.7	1.0003	66.7	1.0002	15.3	37.44
SteinbauerAPM0801 1	R	0.00688	54.16	0.00682	55.56	0.00668	46.88	0.00680	44.03	0.00730	60.00	0.00664	1.0001	0.00941	1.0002	0.00682	48.53
SteinbauerAPM0801 2	R	0.05800	55.77	0.06186	1.13	0.06048	1.00	0.05812	50.62	0.05950	2.30	0.05787	1.1421	0.06652	1.0396	0.05804	52.64
SteinbauerAPM0801 3	R	0.00621	54.53	0.00722	55.56	0.00611	48.88	0.00611	45.41	0.00765	60.00	0.00701	1.0001	0.00987	1.0003	0.00614	49.44
SteinbauerAPM0801 4	R	0.0040	7.40	0.0040	7.18	0.0037	5.70	0.0038	6.26	0.0035	14.00	0.0032	1.0045	0.0044	1.0011	0.0038	6.39
ThomaIMT0400	R	0.005	1.03	0.005	1.06	0.012	0.70	0.028	1.00	0.014	1.61	0.020	1.4199	0.024	1.137	0.013	1.00
KavakAsilomar98	S	0.0151	2.11	0.0153	2.04	0.0045	1.59	0.0020	1.71	0.0116	3.76	0.0346	1.0841	0.1806	1.023	0.0024	1.88
KleinISSTA96 2	S	0.16	4.76	0.16	4.76	0.10	3.36	0.11	3.70	0.07	8.10	0.04	1.0181	0.35	1.0042	0.13	4.06
MogensenVTC97	S	0.052	5.56	0.052	5.56	0.029	3.75	0.033	4.10	0.022	8.81	0.016	1.0162	0.202	1.0045	0.040	4.48
TakadaJSAC0402	S	0.100	6.26	0.100	6.25	0.068	4.72	0.077	5.06	0.061	11.61	0.056	1.0085	0.225	1.0021	0.084	5.55
ZhuAPSIS00	S	0.170	13.81	0.172	13.89	0.112	9.72	0.129	10.34	0.100	23.24	0.099	1.0022	0.582	1.0007	0.148	11.03
DeJongVTC99F 1	U	0.0179	4.14	0.0187	4.03	0.0181	2.78	0.0183	3.06	0.0176	6.67	0.0162	1.0226	0.0186	1.0048	0.0183	3.06
DeJongVTC99F 2	U	0.0048	3.08	0.0048	3.02	0.0040	2.22	0.0043	2.37	0.0035	5.52	0.0026	1.0288	0.0051	1.0061	0.0045	2.67
FleuryJSAC0399 1	U	0.0602	4.77	0.0604	4.76	0.0242	3.60	0.0304	3.88	0.0178	8.51	0.0123	1.0171	0.2474	1.0042	0.0383	4.30
FleuryJSAC0399 2	U	0.0075	9.46	0.0075	9.35	0.0071	6.69	0.0073	7.39	0.0069	16.23	0.0061	1.0043	0.0068	1.0007	0.0073	7.92
KleinISSTA96 3	U	0.0801	1.61	0.0803	1.62	0.0556	1.27	0.0643	1.33	0.0489	3.25	0.0326	1.0866	0.1544	1.2388	0.0696	1.45
KlochAPT0901	U	0.0152	0.81	0.0181	1	0.0184	0.55	0.0575	1.00	0.0193	1.27	0.0223	1.6244	0.024	1.2265	0.0393	1.00
LaurilaAPT0202	U	0.57	2.44	0.57	2.44	0.51	2.09	0.53	2.13	0.50	5.28	0.45	1.0280	0.84	1.0867	0.55	2.30
PedersenVTT0300	U	0.147	5.14	0.148	5.15	0.034	3.87	0.055	4.17	0.015	9.22	0.021	1.0141	0.688	1.0034	0.080	4.62
TanakaJSAC0800	U	3.8051	37.89	4.1482	37.04	2.0775	29.99	2.5035	32.36	2.0362	60.00	0.7669	1.0003	21.8894	1.0001	2.9061	55.51
ZhuVTC01S	U	0.0030	1.38	0.0030	1.39	0.0010	1.01	0.0005	1.09	0.0020	2.37	0.0065	1.2033	0.0363	1.0623	0.0008	1.21

Table 5.1: Least-Square Errors for "Geometrical Models" with empirical datatsets

5.1.1 Empirical Measurement Environment Settings

In addition to calibrating the models to determine which models best fit the empirical measurements, we also need to classify which models are best suited for particular environment settings. In order to determine which geometric models fit which environments the best, we need to classify all empirical datasets into three different environment settings. The characteristics of these typical environment settings are described as below:

Rural (R) - The rural environment consists of flat or hilly terrain (possibly surrounded by large hills or mountains). There are very few buildings or no buildings in the surrounding environment. The landscape may also contain large amounts of vegetation such as forests and meadows. Typically, the rural setting has large open spaces and is characterized by the natural surrounding environment.

Suburban (S) - The suburban environment consists of small buildings of approximately 3 to 5 stories in height. The landscape may also contain scattered vegetation in areas such as parks. There is significanly less amounts of open space compared to a rural environment settings. Residential communities are typical examples of a suburban setting.

Urban (U) - The urban environment is best depicted by dense downtown areas of large metropolitan cities. This setting has large tall high rise buildings greater than 5 stories. This includes office skyscrapers, apartment buildings, high rise hotels, and high rise towers. Secondly, there is no open space due to the dense build up and narrow streets.

The following paragraph describes the environment setting in which each empirica dataset was obtained. It also describes the height of the MS and BS antenna, whether the measurement was taken in the Line of Sight(LOS) of the BS, and the frequency used in the measurements. Since all empirical data has been taken from conference and journal papers, the environment and parameters used are not always explicitly stated. In such cases the parameter value is not known.

Reference	Setting	Location	Environment	BS Ant. Height (m)	MS Ant. Height (m)	LOS	Frequency (Ghz)
KleinISSTA96 1	Rural	Munich, Germany	slightly hilly, forest and meadows	12.3	unknown	unknown	1.84
MatthewsICMPRC89 1	Rural	Meenwood Valley, U.K.	open site, valley area flats, and few buildings	90	87	Yes	0.87
MatthewsICMPRC89 2	Rural	Meenwood Valley, U.K.	open site, valley area flats, and few buildings	50	87	No	0.87
PedersenVTC98	Rural	Vendsyssel, Denmark	unknown terrain	47	unknown	Yes	unknown
SteinbauerAPM0801 1 2	Rural	Not Applicable	outdoor courtyard, 30m x 30m very few obstacles such as trees no buildings but small structures	unknown	unknown	Yes	5.2
SteinbauerAPM0801 3 4	Rural	Not Applicable	outdoor courtyard, 30m x 30m very few obstacles such as trees no buildings but small structures	unknown	unknown	No	5.2
ThomaIMT0400	Rural	unknown	unknown	unknown	unknown	No	5.2
KavakAsilomar98	Suburban	Austin, Texas, USA	University of Texas campus no high buildings/structures	20	unknown	Yes	1.89
KleinISSTA96 2	Suburban	Munich, Germany	flat terrain, partly built-up area,residential homes	25.8	unknown	unknown	1.84
MogensenVTC97	Suburban	Aalborg, Denmark	irregular street layout 3-5 story buildings few higher buildings	41	unknown	unknown	1.8
TakadaJSAC0402	Suburban	Yokosuka, Japan	residential area, 8m wooden houses	4.4	2.7	No	8.45
ZhuAPSIS00	Suburban	Yokosuka, Japan	residential area, 8m wooden houses	4.4	2.7	No	8.45
DeJongVTC99F 1 2	Urban	Bern and Freiburg, Switzerland	3 to 4 storey buildings scattered vegetation moderate traffic density	5.5	2	No	2
FleuryJSAC0399 1 2	Urban	Aalborg University, Denmark	downtown area 2 storey buildings	7.7	unknown	No	unknown
KleinISSTA96 3	Urban	Munich, Germany	densely build-up area 6 to 8 stories, narrow streets	37.5	unknown	unknown	1.84
KlochAPT0901	Urban	Aalborg University, Denmark	downtown area 2 storey buildings	4	unknown	unknown	1.845
LaurilaAPT0202	Urban	Helsinki, Finland	downtown area, dense buildings, towers, & street canyons	10	unknown	No	2.154
PedersenVTT0300	Urban	downtown Aarhus, Denmark	4-6 story buildings irregular street layout	32	unknown	No	1.8
TanakaJSAC0800	Urban	Tokyo, Japan	apartment, office buildings	50	2.9	No	1.9905
ZhuVTC01S	Urban	Tokyo, Japan	university campus 10 to 57m buildings	4.4	3	Yes	8.45

Table 5.2: Propagation and Measurement Environment for empirical datatsets

Reference	Setting	Best Model	2nd Best	3rd Best
KleinISSTA96 1	Rural	Ellipse	Gaussian	Conical
MatthewsICMPRC89 1	Rural	Gauusian	Conical	Inv. Parab
MatthewsICMPRC89 2	Rural	Ellipse	Conical	Gaussian
PedersenVTC98	Rural	Ellipse	Gaussian	Conical
SteinbauerAPM0801 1 2	Rural	Ellipse	Conical	Inv. Parab
SteinbauerAPM0801 3 4	Rural	Inv Parab	Conical	Gaussian
ThomaIMT0400	Rural	Hollow	Circular disc	Conical
KavakAsilomar98	Suburban	Inv Parab	3D Spheroid	Conical
KleinISSTA96 2	Suburban	Ellipse	Gaussian	Conical
MogensenVTC97	Suburban	Ellipse	Gaussian	Conical
TakadaJSAC0402	Suburban	Ellipse	Gaussian	Conical
ZhuAPSIS00	Suburban	Ellipse	Gaussian	Conical
DeJongVTC99F 1 2	Urban	Ellipse	Gaussian	Circular disc
FleuryJSAC0399 1 2	Urban	Ellipse	Gaussian	Conical
KleinISSTA96 3	Urban	Ellipse	Gaussian	Conical
KlochAPT0901	Urban	Circular disc	Hollow	Conical
LaurilaAPT0202	Urban	Ellipse	Gaussian	Conical
PedersenVTT0300	Urban	Gaussian	Ellipse	Conical
TanakaJSAC0800	Urban	Ellipse	Gaussian	Conical
ZhuVTC01S	Urban	Inv Parab	3D Spheroid	Conical

Table 5.3: Best three models compared against empirical datatsets

5.1.2 Conclusions

From the Table 5.3, we can observe that the uniform Elliptical model is clearly the best model in all environment settings; rural, suburban, and urban. The Gaussian and Conical models are also models in which the empirical data matches closely. The reason that the elliptical and gaussian models give better results when calibrating with empirical data is due to their scatterer distributions. In the elliptical model, the base station and mobile station are enclosed in an elliptical disc. The gaussian model also has the base station and mobile station enclosed by scatterers. Therefore, the AOA at the base station is incident from all directions. Secondly, since many of the empirical datasets have an AOA greater than 90 degrees, these two models are calibrated resulting in the minimum LSE values.

The Elliptical model with more spatially spread scatterers than all other models is best

2/3 of all empirical data sets (18 out of 27). Elliptical is best for rural, suburban, and urban. This is perhaps because of the unavoidability of scatters local to the base station. Elliptals fitnees is especially pronounce over its closes competitor (by over 1/3 in LSE) in urban areas where local scattering around the base station is especially problematic.

One can also observe when calibrating empirical datasets, KlochAPT0901, MatthewICM-PRC89, ZhaoJSAC0402, and SteinbauerAPM0801 (1, 3, & 4), the conical and circular models have a parameter value that is less than one. In such cases, parameter allows the model to be calibrated such that the scatterer distribution encloses the base station. This results in a smaller LSE value.

Other geometric models, such as the inverted parabola and hollow circular disc, have scatterers distributed around the mobile station only. The inverted parabolic model results in the best match for empirical datasets ZhuVTC01S and KavakAsilomar98. The hollow disc model results in the optimal match for ThomaIMT0400.

There seems to be little advantage in having a hollow disc of scatterers over the circular disc. These two models have comparable LSE. The Hollow disc model beats Circular disc model in 1 out of 9 rural datasets, 2 out of 7 suburban datasets, and 1 out of 11 urban datasets. A total of 4 out of 27 for all datasets.

Inverted Parabola is typically worse than conical. The 2 have comparable LSE for rual and suburn, but inverted parabola has notable worse LSE for urban. It also has lower LSE then conical only in 2 out of 7 sub, out of 11 datase , 5 out of 27 overall. Inv parab is worse than conical because the latters scattereres are much more spread out spatially from the center of the mobile.

From Table 4, and Table 5, there is no direct correlation between a specific geometric model and the empirical datasets' carrier frequency, and base station and mobile station heights.

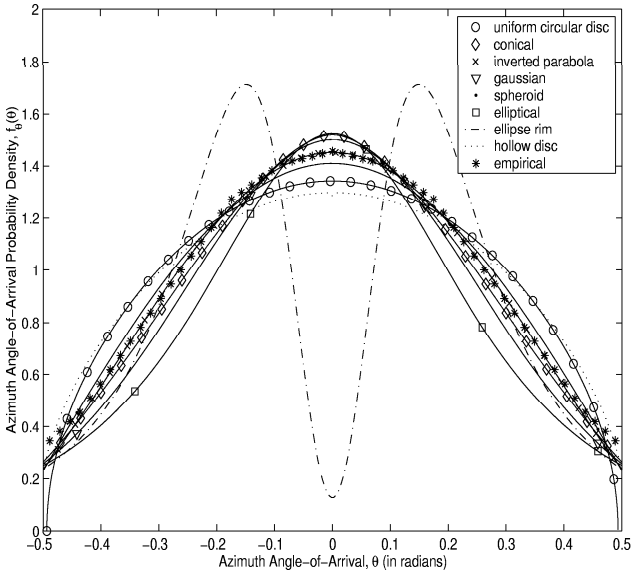

Figure 5.1a: KavakAsilomar98

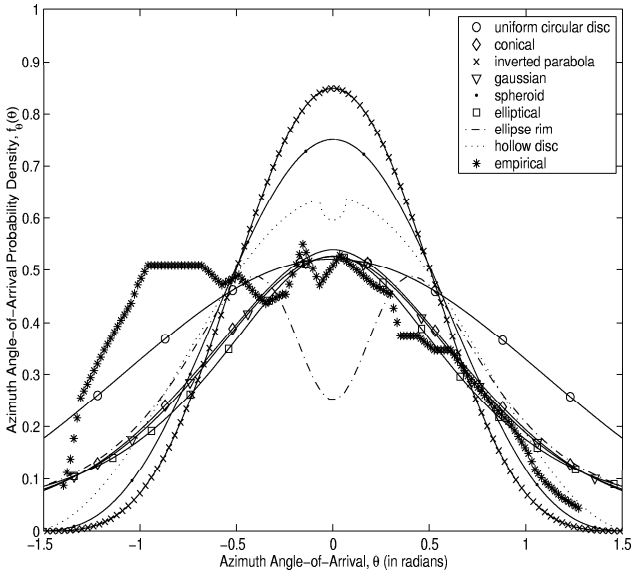

Figure 5.1b: KlochAPT0901

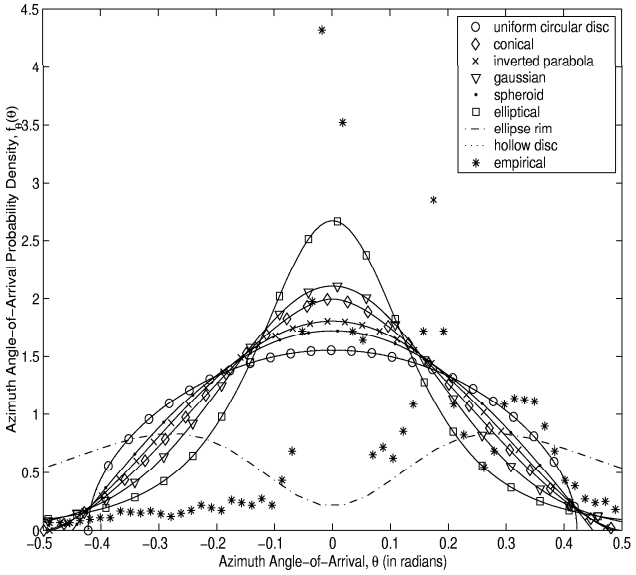

Figure 5.1c: LaurilaAPT0202

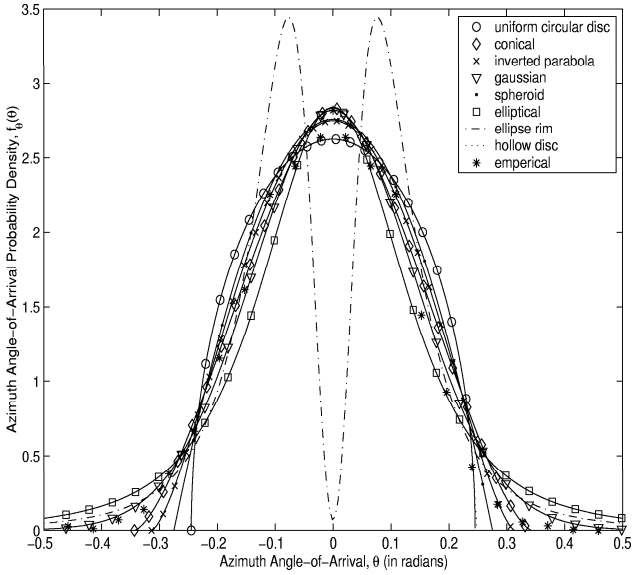

Figure 5.1d: MatthewsICMPRC89

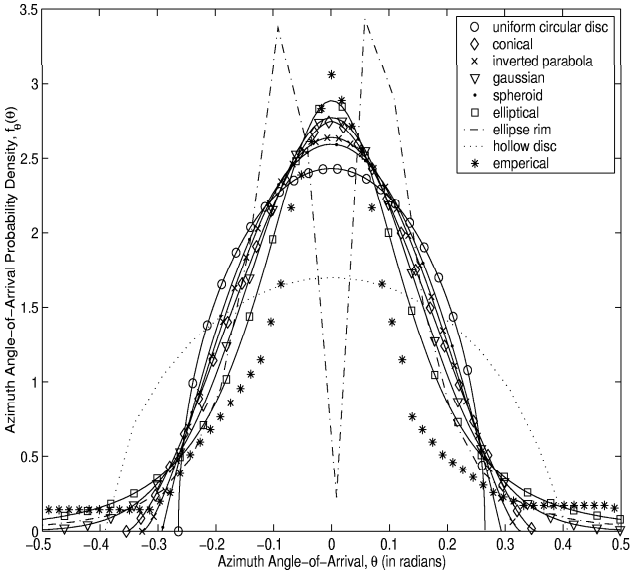

Figure 5.2a: KleinISSSTA96

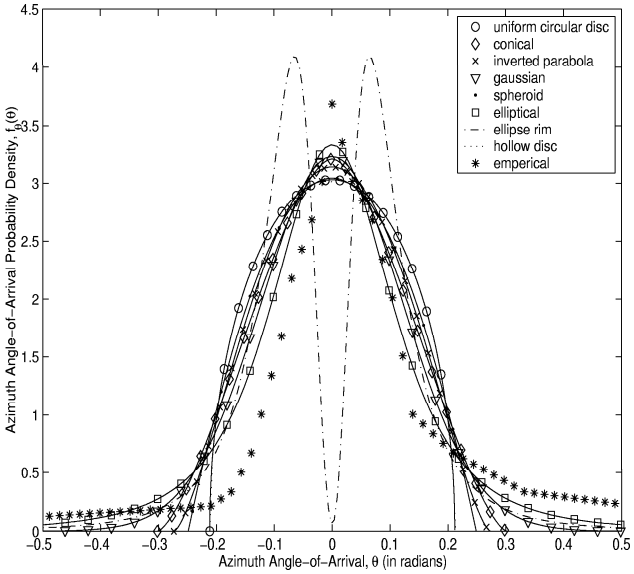

Figure 5.2b: KleinISSSTA96

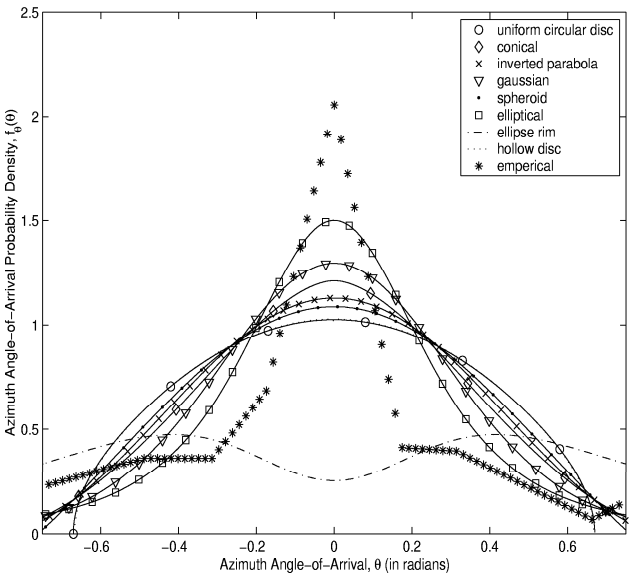

Figure 5.2c: KleinISSSTA96

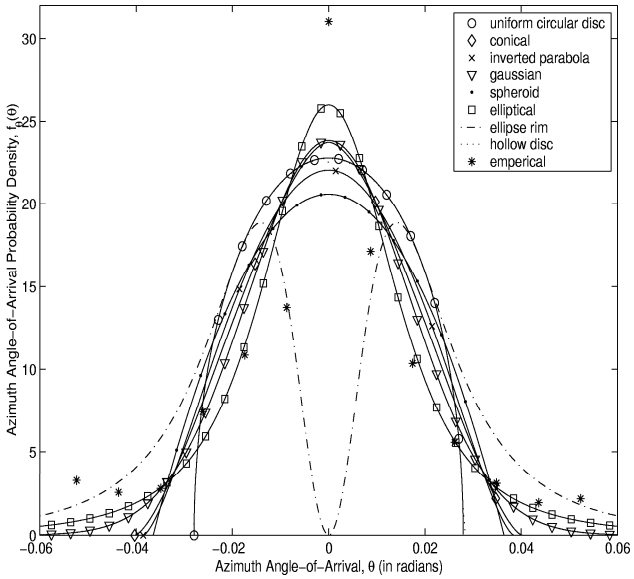

Figure 5.2d: PedersenVTC98

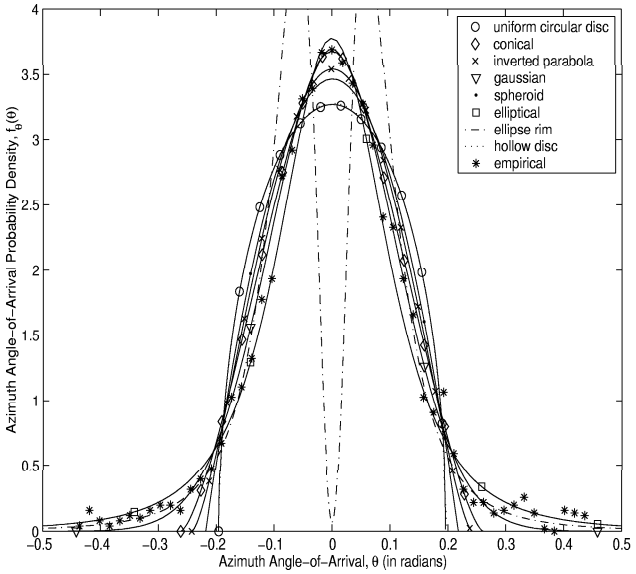

Figure 5.3a: PedersenVTT0300

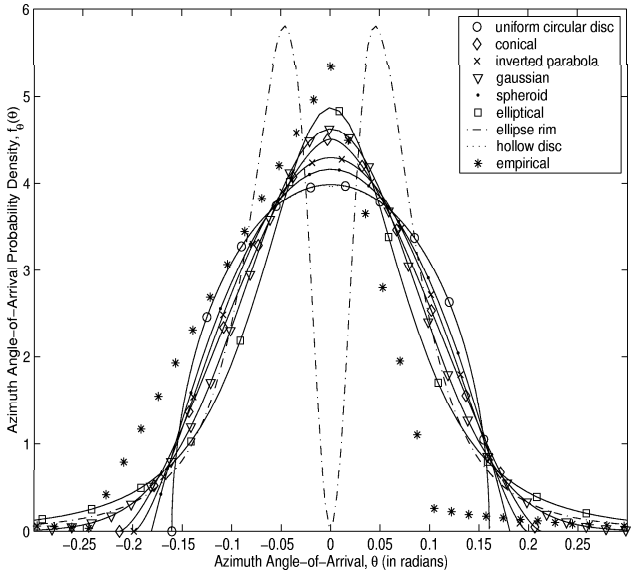

Figure 5.3b: TakadaJSAC0402

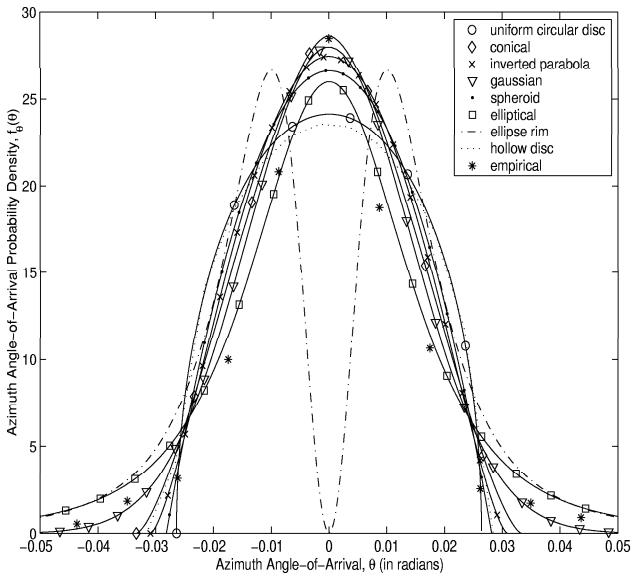

Figure 5.3c: TanakaJSAC0800

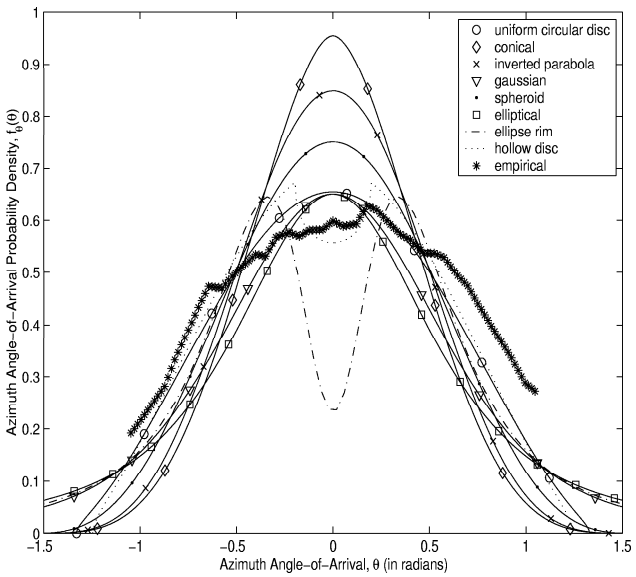

Figure 5.3d: ThomaIMT0400

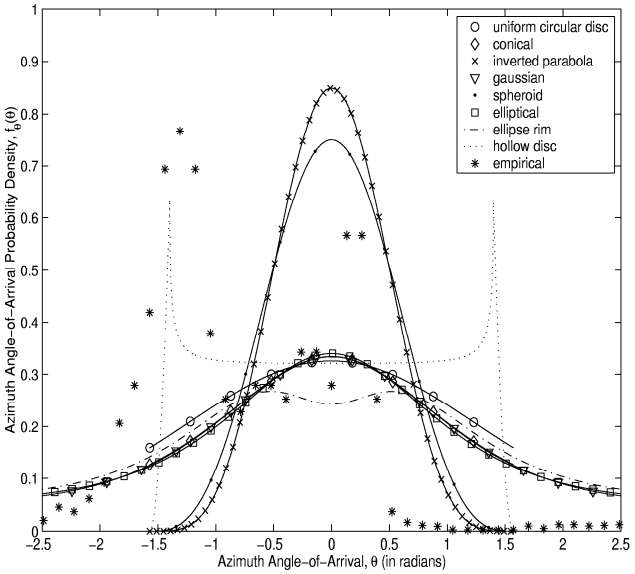

Figure 5.4a: ZhaoJSAC0402

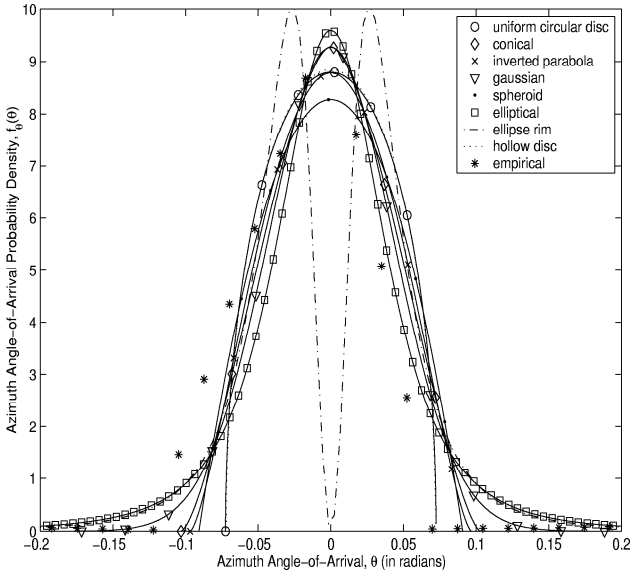

Figure 5.4b: ZhuAPSIS00

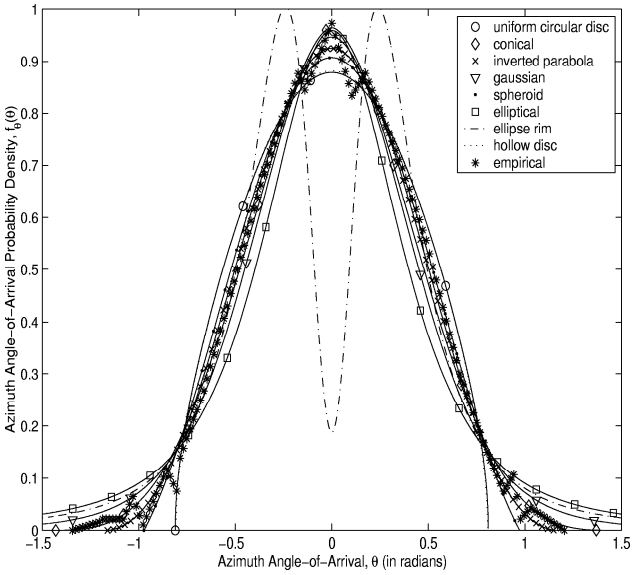

Figure 5.4c: ZhuVTC01S

Bibliography

[1] A. M. D. Turkmani & J. D. Parsons, "Characterisation of Mobile Radio Signals: Base Station Crosscorrelation," *IEE Proceedings: Communications, Speech & Vision*, part I, vol. 138, no. 6, pp. 557-565, December 1991.

[2] P. Zetterberg & B. Ottersten, "The Spectrum Efficiency of a Base Station Antenna Array System for Spatially Selective Transmission," *IEEE Transactions on Vehicular Technology*, vol. 44, no. 3, pp. 651-660, August 1995.

[3] J. C. Liberti & T. S. Rappaport, "A Geometrically Based Model for Line-of-Sight Multipath Radio Channels," *IEEE Vehicular Technology Conference*, pp. 844-848, 1996.

[4] P. Petrus, J. H. Reed & T. S. Rappaport, "Effects of Directional Antennas at the Base Station on the Doppler Spectrum," *IEEE Communications Letters*, vol. 1, no. 2, pp. 40-42, March 1997.

[5] P. C. F. Eggers, "Generation of Base Station DOA Distribution by Jacobi Transformation of Scattering Areas," *IEE Electronics Letters*, vol. 34, no. 1, pp. 24-26, January 8, 1998.

[6] O. Norklit & J. B. Andersen, "Diffuse Channel Model and Experimental Results for Array Antennas in Mobile Environments," *IEEE Transactions on Antennas & Propagation*, vol. 46, no. 6, pp. 834-840, June 1998.

[7] R. J. Piechocki, G. V. Tsoulos & J. P. McGeehan, "Simple General Formula for PDF of Angle of Arrival in Large Cell Operational Environments," *IEE Electronics Letters*, vol. 34, no. 18, pp. 1784-1785, September 3, 1998.

[8] D. R. Van Rheeden & S. C. Gupta, "A Geometric Model for Fading Correlation in Multipath Radio Channels," *IEEE International Conference Communications*, pp. 1655-1659, 1998.

[9] S. Roy, "A Three-Dimensional Wideband Propagation Model for the Study of Base Station Antenna Arrays with Application to LMCS," *IEEE Vehicular Technology Conference*, pp. 1805-1809, 1998.

[10] J. Laurila, A. F. Molisch & E. Bonek, "Influence of the Scatterer Distribution on Power Delay Profiles and Azimuthal Power Spectra of Mobile radio Channels," *International Symposium Spread Spectrum Technology & Applications*, pp. 267-271, 1998.

[11] S. Y.-D. Lien & M. Cherniakov, "Analytical Approach for Multipath Delay Spread Power Distribution," *IEEE Global Telecommunications Conference*, pp. 3680-685, 1998.

[12] S. Qu & T. Yeap, "A Three-Dimensional Scattering Model for Fading Channels in Land Mobile Environment," *IEEE Transactions on Vehicular Technology*, vol. 48, no. 3, pp. 765-781, May 1999.

[13] S.-T. Kim, J.-H. Yoo & H.-K. Park, "A Spatially and Temporally Correlated Fading Model for Array Antenna Applications," *IEEE Transactions on Vehicular Technology*, vol. 48, no. 6, November 1999.

[14] J.-K. Han, C. Mun & H.-K. Park, "A Deterministic Fading Channel Model with Rigorous Correlation Characteristics," *IEEE Vehicular Technology Conference*, pp. 122-126, Fall 1999.

[15] M. P. Lotter & P. van Rooyen, "Modeling Spatial Aspects of Cellular CDMA/SDMA Systems," *IEEE Communications Letters*, vol. 3, no. 5, pp. 128-131, May 1999.

[16] R. Narasimban & D. C. Cox, "A Generalized Doppler Power Spectrum for Wireless Environments," *IEEE Communications Letters*, vol. 3, no. 6, pp. 164-165, June 1999.

[17] R. B. Ertel & J. H. Reed, "Angle and Time of Arrival Statistics for Circular and Elliptical Scattering Models," *IEEE Journal on Selected Areas in Communications*, vol. 17, no. 11, pp. 1829-1840, November 1999.

[18] K. I. Pedersen, P. E. Mogensen & B. H. Fleury, "A Stochastic Model of the Temporal and Azimuthal Dispersion Seen at the Base Station in Outdoor Propagation Environments," *IEEE Transactions on Vehicular Technology*, vol. 49, no. 2, pp. 437-447????, March 2000.

[19] A. Abdi & M. Kaveh, "A Versatile Spatio-Temporal Correlation Function for Mobile Fading Channels with Non-isotropic Scttering," *IEEE IEEE Signal Processing Symposium on Sensor & Adaptive Processing*, pp. 58-62, 2000.

[20] P. Petrus, J. H. Reed & T. S. Rappaport, "Geometrical-based Statistical Macrocell Channel Model for Mobile Environments," *IEEE Transactions on Communications*, vol. 50, no. 3, pp. 495-502, March 2002.

[21] R. Janaswamy, "Angle and Time of Arrival Statistics for the Gaussian Scatter Density Model," *IEEE Transactions on Wireless Communications*, vol. 1, no. 3, pp. 488-497, July 2002.

[22] Y. Z. Mohasseb & M. P. Fitz, "A 3-D Spatio-Temporal Simulation Model for Wireless Channel," *IEEE Journal on Selected Areas in Communications*, vol. 20, no. 6, pp. 1193-1203, August 2002.

[23] R. Janaswamy, "Angle of Arrival Statistics for a 3D Spheroid Model," *IEEE Transactions on Vehicular Technology*, vol. 51, no. 5, pp. 1242-1247, September 2002.

[24] A. Y. Olenko, K. T. Wong & E. H.-O. Ng, "Analytically Derived TOA-DOA Statistics of Uplink/Downlink Wireless Multipaths Arisen from Scatterers on an Hollow-Disc Around the Mobile," *IEEE Antennas & Wireless Propagation Letters*, vol. 2, issue 22, pp. 345-348, 2003.

[25] A. Y. Olenko, K. T. Wong & M. Abdulla, "Analytically Derived TOA-DOA Statistics of Uplink/Downlink Wireless-Cellular Multipaths Arisen from Scatterers with an Inverted-Parabolic Spatial Distribution Around the Mobile," submitted to the *IEEE Signal Processing Letters*.

[26] A. Velazquez, D. Covarrubias & A. Zamora, "On Selecting Alternative Service Zones by Using a New Double Elliptical Scattering Model in Smart Antenna Systems," submitted to *IEEE Transactions on Antennas & Propagation*.

[27] A. Klein & W. Mohr, "A Statistical Wideband Mobile Radio Channel Model Including the Directions-of-Arrival," *IEEE International Symposium Spread Spectrum Technology and Applications* pp. 102-106, 1996.

[28] P. A. Matthews, D. Molkdar & B. Mohebbi, "Diection of Arrival and Frequency Response Measurements at UHF," *ICMRPC ????????????* 1989.

[29] K. I. Pedersen, P. E. Mogensen & B. H. Fleury, "Spatial Channel Characteristics in Outdoor Environments and Their Impact on BS Antenna System Performance," *IEEE Vehicular Technology Conference*, pp. 719-723, 1998.

[30] M. Steinbauer, A. F. Molisch & E. Bonek, "the Double-Directional Radio Channel," *IEEE Antennas & Propagation Magazine*, vol. 43, no. 4, pp. 51-63, August 2001.

[31] R. S. Thoma, D. Hampicke, A. Richter, G. Sommerkorn, A. Schneider, U. Trautwein & W. Wirnitzer, "Identification of Time-Variant Directional Mobile Radio Channels," *IEEE Transactions on Instrumentation & Measurement*, vol. 49, no. 2, pp. 357-364, April 2000.

[32] P. E. Mogensen, K. I. Pedersen, P. Leth-Espensen, B. Fleury, F. Frederiksen, K. Olesen & S. L. Larsen, "Preliminary Measurement Results from an Adaptive Antenna Array Testbed for GSM/UMTS," *IEEE Vehicular Technology Conference*, pp. 1592-1596, 1997.

[33] J.-I. Takada, J. Fu, H. Zhu & T. Kobayashi, "Spatio-Temporal Channel Characterization in a Suburban Non Line-of-Sight Microcellular Environment," *IEEE Journal on Selected Areas in Communications*, vol. 20, no. 3, pp. 532-538, April 2002.

[34] B. H. Fleury, M. Tschudin, R. Heddergott, D. Dahlhaus & K. I. Pedersen, "Channel Paremter Estimation in Mobile Radio Environments Using the SAGE Algorithm," *IEEE Journal on Selected Areas in Communications*, vol. 17, no. 3, pp. 434-450, March 1999.

[35] C. Kloch, G. Liang, J. B. Andersen, G. F. Pedersen & H. L. Bertoni, "Comparison of measured and Predicted Time Dispersion and Direction of Arrival for Multipath in a Small Cell Environment," *IEEE Transactions on Antennas & Propagation*, vol. 49, no. 9, pp. 1254-1263, September 2001.

[36] J. Laurila, K. Kalliola, M. Toeltsch, K. Hugl, P. Vainikainen & E. Bonek, "Wide-Band 3-D Characterization of Mobile Radio Channels in Urban Environment," *IEEE Transactions on Antennas & Propagation*, vol. 50, no. 2, pp. 233-243, February 2002.

[37] K. I. Pedersen, P. E. Mogensen & B. H. Fleury, "A Stochastic Model of the Temporal and Azimuthal Dispersion Seen at the Base Station in Outdoor Propagation Environments," *IEEE Transactions on Vehicular Technology*, vol. 49, no. 2, pp. 437-447, March 2000.

[38] S. Tanaka, A. Harada, M. Sawahasji & F. Adachi, "Experiments on Coherent Adaptive Antenan Array Diversity for Wideband DS-CDMA Mobile Radio," *IEEE Journal on Selected Areas in Communications*, vol. 18, no. 8, pp. 1495-1504, August 2000.

[39] H. Zhu, J. Fu, K. Araki, H. Masui, M. Ishii, K. Sakawa, H. Shimizu, T. Kobayahsi, "A Spactio-Temporal Channel Measurement and Ray-Tracing Validation in Suburban Microcell Environments," *APSIS* , pp. 1138-1141, 2000.

[40] H. Zhu, J. Takada, T. Kobayahsi, "The Verification of a deterministic Spatio-Temporal Channel Modeling Approach by Applying a Deconvolution Technique in the Measurement," *IEEE Vehicular Technology Conference*, pp. 362-366, 2001.

[41] Y. L. C. de Jong, M. H. A. J. Herben, "Experimental Verification of Ray-Tracing Based Propagation Prediction Models for Urban Microcell Environments," *IEEE Vehicular Technology Conference*, pp. 1434-1438, 1999.

Appendix A

Rayleigh vs Gaussian Scatterer Distributions

The rayleigh scatterer distribution around the MS proposed and derived by Laurila [10] makes an assumption that $D >> \sigma$. The closed form expression for the AOA probability density function of this geometric model takes into account this assumption in its derivation. As a result, values where the ratio, D/σ, are not large cannot be used as the distribution results in negative values. As an example, the AOA distribution for this scatterer distributions is plotted in Figure A.1a. Secondly, for comparison, we also plot the geometric model with a gaussian scatterer distribution proposed by Janaswamy [21]. It is clearly seen that the AOA distribution for the rayleigh scatterer distribution is not correct as it contains negative values. However, when large values are used, the assumption assumed by Laurila is true and the AOA distribution matches very closely to the gaussian geometric model derived by Janaswamy. If we compute the lease square error (LSE) between the AOA distribution's for various values of D/σ, we obtain Figure A.1b. Due to the inconsistency in the rayleigh model, we have used the gaussian model instead which

has the correct AOA distribution for all values of D/σ.

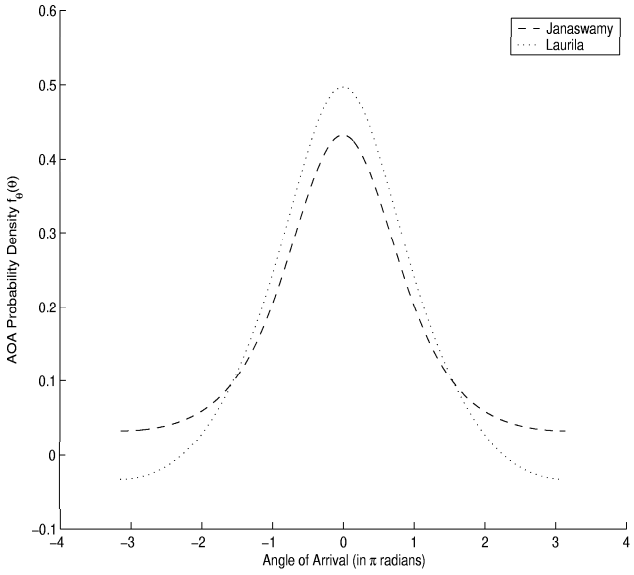

Figure A.1a: Rayleigh vs Gaussian Distribution for $D/\sigma = 1$

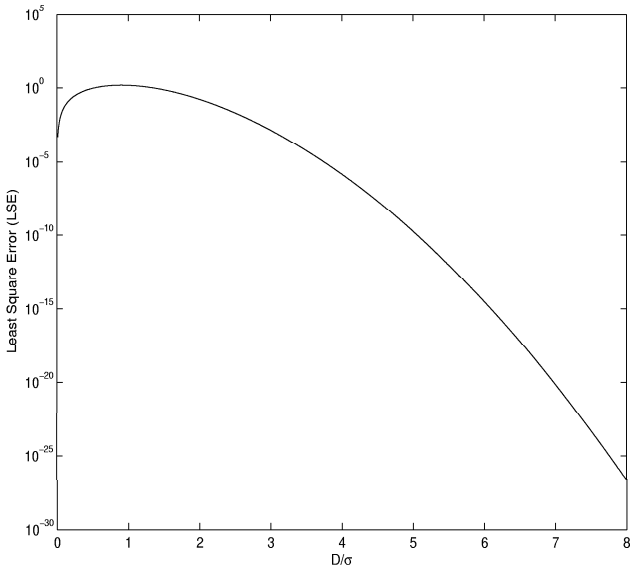

Figure A.1b: LSE for various values of D/σ

Appendix B

AOA Distribution Fitting using AOA spread

The following table summarizes various empirical papers' measured AOA spreads and each geometric model's corresponding parameter giving this same AOA spread. See Figures B.1a,B.1b, B.1c,B.1d,B.1e,B.1f for comparison between empirical data and specific geometric models.

Reference	AOA Spread	3D Spheriod D/R	Hollow Disc $r = 0.1 * R$	$r = 0.5 * R$	$r = 0.99 * R$	Inv. Parabola D/R	Gaussian σ/D	Conical D/R	Circular D/R
ThomaIMT0400	30.7°	1*	1.047	1.1364	1.3514	NA	0.4505	1	1
LaurilaAPT0202	8.8687°	2.9	3.2258	3.5714	4.3478	2.66	0.1529	2.6	3.3
PedersenVTT0300	7.01°	3.6	4.1667	4.5455	5.2632	3.4	0.122	3.2	4
KlochAPT0901	38.65°	1*	1*	1*	1.1494	NA	0.1215	0.59	0.9091
TanakaJSAC0800	1.099°	23.3	26.31	29.4	34.482	21.29	0.0192	NA	26
FleuryJSAC0399	9.1749°	2.8	3.1546	3.5088	4.1152	2.57	0.158	2.45	3.2

Table B.1: Parameters corresponding to angular spread for "Geometrical Models"

* - In these models, the AOA spread exceeds the maximum AOA spread of the model. Since the maximum AOA spread occurs when D/R is a minimum, this minimum value of 1 is used. Therefore, the geometric-model parameter which produced this maximum angular spread was used.

NA - In these models, the geometric-model AOA spread was outside the range of all possible empirical AOA spread values for a given parameter. Therefore, this model could not be compared with the empirical dataset.

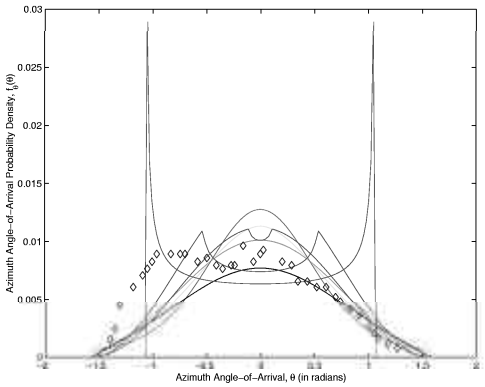

Figure B.1a: AOA KlochAPT0901

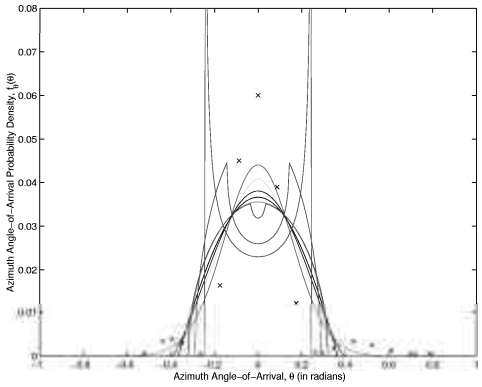

Figure B.1b: AOA FleuryJSAC0399

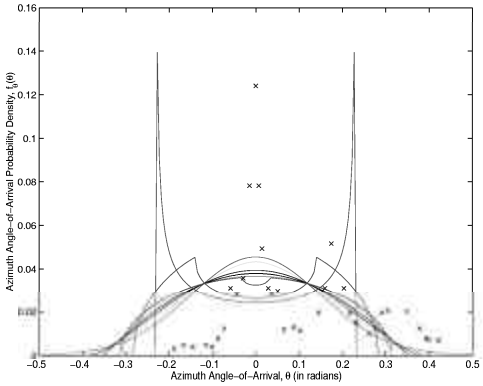

Figure B.1c: AOA LauriLaAPT0202

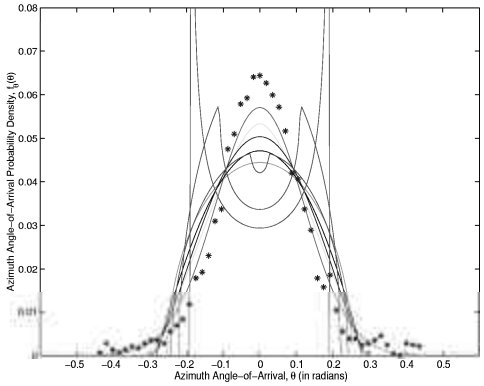

Figure B.1d: AOA PedersenVTT0300

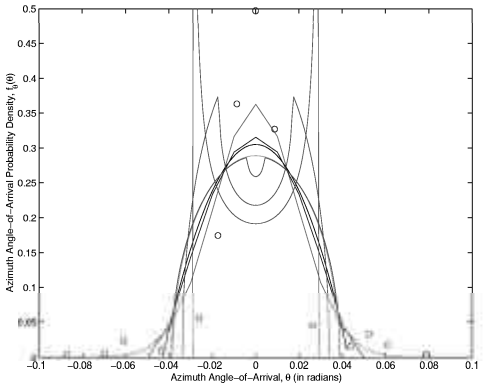

Figure B.1e: AOA TanakaJSAC0800

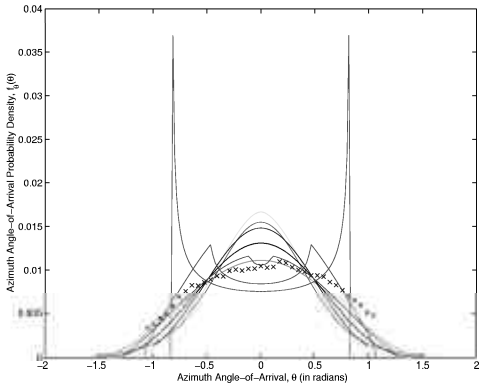

Figure B.1f: AOA ThomaIMT0400

Appendix C

TOA Distributions

TOA Marginal distribution curves:

1) D, D/R, D/σ : As we increase these parameter values, the maximum and minimum delay of the multipath components also increases. Similarly, if we decrease these parameter values, the maximum and minimum arrival delays decrease. This observation is trivial since increasing and decreasing the distance between the MS and BS will result in long and short delay paths respectively. For scatterers uniformly distributed in a circular disc around the MS, the shape of the TOA curve remains the same for all values of D such that the ratio D/R is constant. Only the arrival delay times change w.r.t. D. The TOA curve derived in [ErtelJSAC1199] does not show this property. The reason for this anomality could be due to an error in the original derivation by the authors.

2) r/R: This parameter is used only in the hollow disc scatterer distribution model. When r/R approaches 0, we obtain a circular disc of scatteres and the DOA curve reduces to the uniform scatterer distribution model. When r/R approaches unity,

the curve peaks at the minimum and maximum delay arrival times.

C.0.3 TOA models vs empirical data

The time of arrival(TOA) was another channel fading metric measured in an outdoor enviroment setting. Similar to DOA mentioned in the previous section, the second order statistics, delay spread was numerically calculated for all models and empirical datasets[1]. From this delay spread, each geometric TOA model was calibrated to determine model parameters. Unlike the DOA models, in order to properly calibrate models, we must have a priori knowledge of the distance between the base station and the mobile. The reason for this is due to the fact that the TOA model parameter, D cannot be determined from the delay spread directly.

The following table summarizes the delay spread of empirical data and each geometric models corresponding parameter which also produces the same delay spread.

NA - In these models, the delay spread was outside the range of all possible delay spread values for a given parameter. Therefore, this model could not be compared with the empirical dataset.

See Figures C.1a,C.1b,C.1c,C.1d,C.2a ,C.2b,C.2c,C.2d,C.3a,C.3b for comparison between empirical data and specific geometric models.

A finite support region leads to a fintie maximum in relative delay, as expected.

The hollow-disk support region of [24] allows the TOA distribution a second peak,

[1]The delay spread for the geometric model with uniform scatteres in a circular disc found in ErtelJSAC1199, [17], could not be calculated correctly using numerical integration. The spread values obtained were complex. The reason for this is yet to be determined. As a result, the geometric model with uniform scatterers in a hollow disc was used to calculate the delay spread by setting the parameter value to $r = 0.0001$.

Author, Venue & Date	Delay Spread (in $\mu secs$)	Distance D	Hollow Disc $r = 0.1 * R$	$r = 0.5 * R$	$r = 0.99 * R$	Inv. Parabola D/R	Gaussian D/σ	Circular D/R
ErcegJSAC0399	0.2409	500	4.1322	90.09	12.1	55.5	3.25	8
	0.106	500	NA	NA	NA	NA	7.5	10.8
	0.1173	500	NA	NA	NA	NA	6.75	10.7
	0.1629	500	NA	NA	NA	NA	4.85	10.2
KlochAPT0901	0.0781	72	43	30.69	3.7	18.5	1.45	4.2
KucharAPT0200	0.3205	700	3.7838	128.7	19	85	3.45	0.3, 12.8
LaurilaAPT0202	0.4752	500	1.8519	207.9	27	131	1.65	0.625, 9
SteinbauerAPT0801	0.0307	8	NA	NA	NA	NA	NA	NA
	0.0177	28	NA	NA	NA	NA	2.5	9
	0.0727	28	NA	NA	NA	NA	N/A	1.7
	0.0426	28	1.4	16.83	2	10.5	1.05	3
PedersenVTT0300	0.69	1500	2.4	396	60	275	3.4	9
	0.69	2000	2.5	470.25	80	350	4.5	11.5
	0.69	1750	2.5	420.75	70	312.5	4	10

Table C.1: Parameters corresponding to delay spread for "Geometrical Models"

whose delay-value and height and sharpness may be controlled by r/R.

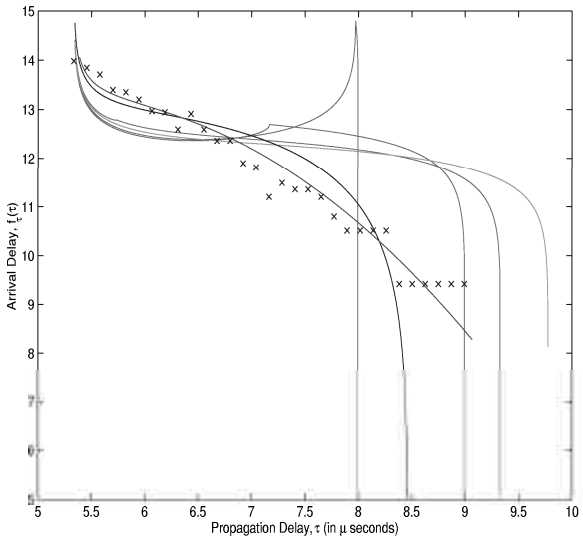

Figure C.1a: TOA PedersonVTT0300 $D = 1500$

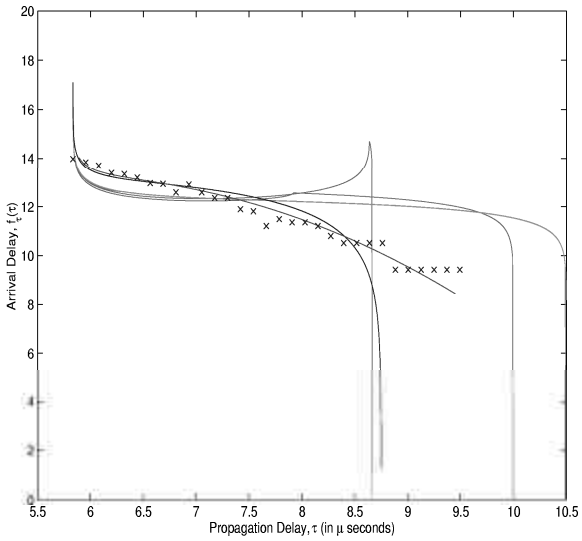

Figure C.1b: TOA PedersonVTT0300 $D = 1750$

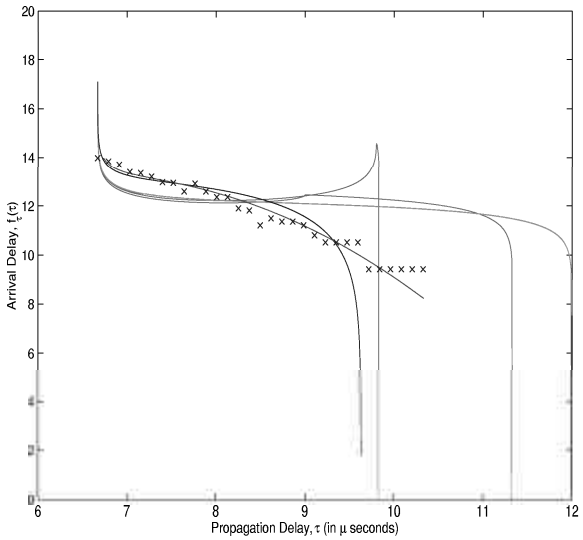

Figure C.1c: TOA PedersonVTT0300 $D = 2000$

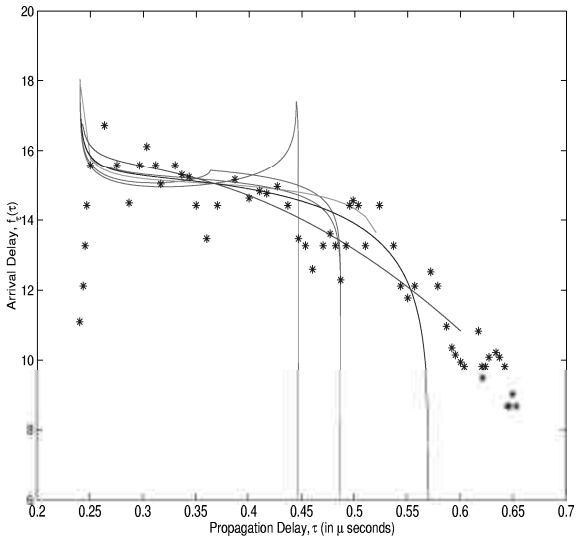

Figure C.1d: TOA KlochAPT0901

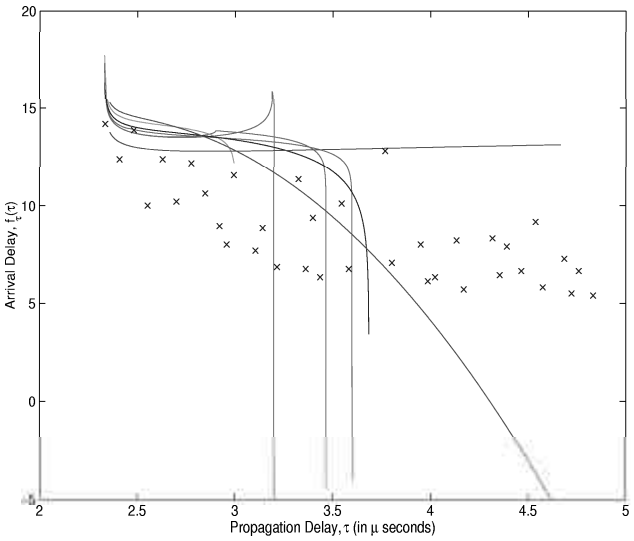

Figure C.2a: TOA KucharAPT0200

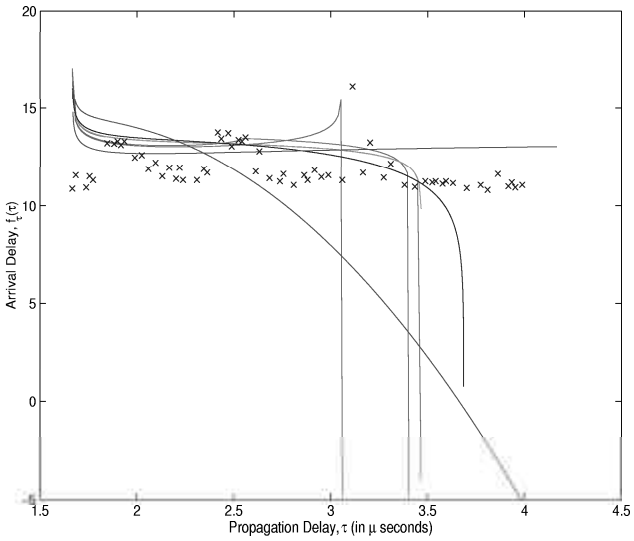

Figure C.2b: TOA LaurilaAPT0202

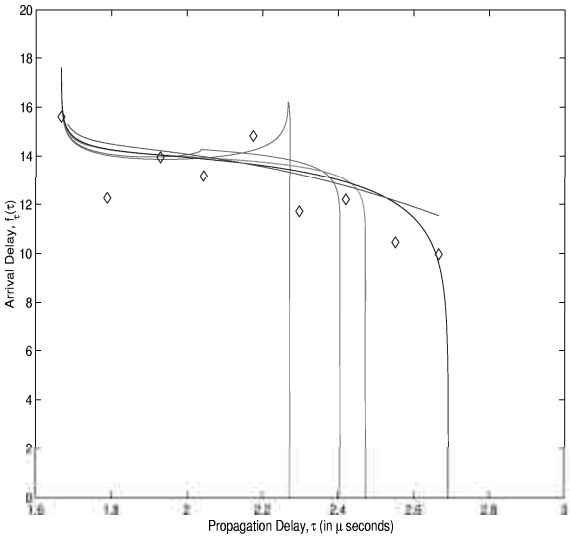

Figure C.2c: TOA ErcegJSAC0399 $D = 500$

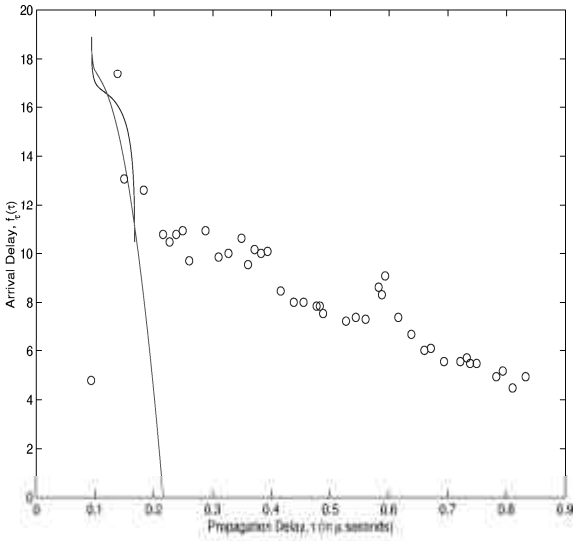

Figure C.2d: TOA SteinbauerAPT0801 Scenario 2.eps

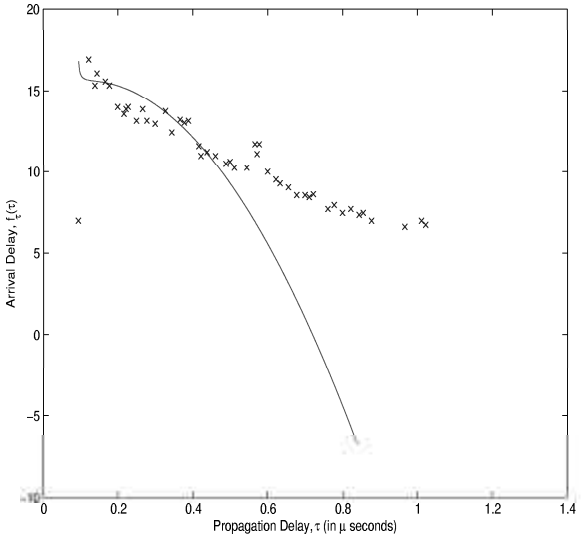

Figure C.3a: TOA SteinbauerAPT0801 Scenario 3.eps

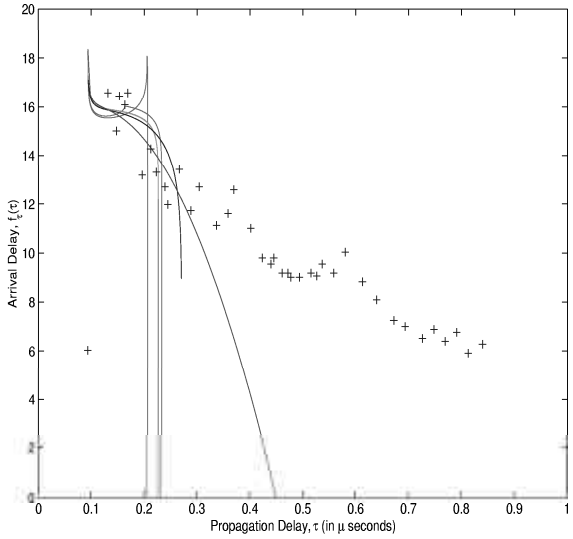

Figure C.3b: TOA SteinbauerAPT0801 Scenario 4.eps